Review—Silicon Nitride and Silicon Nitride-Rich Thin Film Technologies: Trends in Deposition Techniques and Related Applications

Alain E. Kaloyeros,[a] Fernando A. Jové,[b] Jonathan Goff,[b] and Barry Arkles[b,*,z]

[a]*SUNY Polytechnic Institute, Albany, New York 12203, USA*
[b]*Gelest, Inc., Morrisville, Pennsylvania 19067, USA*

This article provides an overview of the state-of-the-art chemistry and processing technologies for silicon nitride and silicon nitride-rich films, i.e., silicon nitride with C inclusion, both in hydrogenated (SiN_x:H and SiN_x:H(C)) and non-hydrogenated (SiN_x and SiN_x(C)) forms. The emphasis is on emerging trends and innovations in these SiN_x material system technologies, with focus on Si and N source chemistries and thin film growth processes, including their primary effects on resulting film properties. It also illustrates that SiN_x and its SiN_x(C) derivative are the focus of an ever-growing research and manufacturing interest and that their potential usages are expanding into new technological areas.

Manuscript submitted June 28, 2017; revised manuscript received September 5, 2017. Published September 29, 2017.

Silicon nitride and carbide thin films, primarily in the form of silicon nitride (SiN_x), silicon carbide (SiC_y), and silicon carbo-nitride (SiN_xC_y), where $0 < x < 1.33$ and $0 < y < 1$, are experiencing a burgeoning of research interest across multiple application sectors. The appeal of these Si-based coatings is attributed to their highly desirable combination of physical, mechanical, electrical, and optoelectronic properties making them prime candidates for applications in the automotive, aerospace, computer chip, solar, light-emitting, and medical industries.[1–6] In consideration of the intense current interest in SiN_x and SiN_xC_y, and the expectation that their applications will continue to witness further expansion and extensive diversification, we present an overview on the latest trends and developments in hydrogenated and non-hydrogenated silicon nitride and silicon carbonitride deposition techniques and associated post-deposition processing technologies. Given the fast-moving nature of SiN_x and SiN_xC_y technological advances, the intent is to present an survey of work published within the last five years for silicon nitride and silicon nitride-rich films, i.e., silicon nitride with C inclusion, both in hydrogenated (SiN_x:H and SiN_x:H(C)) and non-hydrogenated (SiN_x and SiN_x(C)) forms. Prior years reports will be discussed only in the context of providing appropriate background and support for the more contemporary results summarized herein. This article is not intended to be a comprehensive review, but instead is meant to provide the reader with a focused analysis of research directions particularly where, in the authors' experience, they are reflective of potential commercial relevance.

The silicon nitride literature presents a complex picture of its properties: mechanical, thermal, electrical, tribological, etc. In the best cases, the properties are associated with well-defined chemical compositions and morphologies. However, silicon nitride is frequently described by the process by which it is formed, and reported properties are for compositions that are not fully defined. Accordingly, this review is centered on silicon nitride deposition and the processes and selected properties associated with specific modifications in deposition techniques. While a detailed analysis of film physical, chemical, electrical and optical properties over the range of deposition technologies and conditions is not presented herein, salient properties are summarized in tabular form. Analyses of thin film properties as function of most researched deposition techniques, and an evaluation of resulting applications as they pertain to film properties, will be presented in a subsequent review.

For instance, SiN_x, SiC_y, and SiN_xC_y[1–4] are employed as hard protective coatings under challenging thermal, environmental, and chemical conditions due to their high hardness (potentially in excess of 40GPa), effective oxidation resistance, elevated temperature and thermal shock resistance as well as chemical stability, and attractive mechanical, tribological and dielectric properties.[5–9] In particular, bonding in SiN_x, SiC_y, and SiN_xC_y exhibits substantially greater covalent character than in silicon dioxide (SiO_2). SiN_x, SiC_y, and SiN_xC_y can therefore provide an intrinsically greater resistance to diffusive migration than SiO_2, a feature that is of utmost impact at nanoscale dimensions.

Ultrathin films of SiN_x and SiC_y are utilized in a broad spectrum of applications in integrated circuitry (IC) technologies, particularly in the microprocessor unit (MPU), system-on-a-chip (SoC), flash memory, and the vertical stacking of electronic devices in what is commonly referred to as three-dimensional (3D) integrated systems.[10] For one, SiN_x is widely adopted as diffusion barrier for silicon dioxide (SiO_2) dielectric with the introduction of copper metallization structures. Additionally, SiC_y, SiN_xC_y, and SiC_yO_z are applied as diffusion barriers in combination with low dielectric constant (κ) material replacements to SiO_2.[11–13] Similarly, SiN_x and SiN_xC_y are used as capping layers and etch stops for copper interconnects either individually or, more recently, in combination with selective cobalt capping.[14] The dominant low interlevel dielectric (ILD) film for the bottom few metal layers of the MPU is SiOCH, and for flash memory architectures it is SiOC.[10] Other IC applications incorporate SiN_x as a dielectric such as metal-insulator-metal capacitors and thin film transistors (TFTs) due to its high dielectric constant which enables the deposition of thinner films while preserving higher breakdown voltage and lower leakage current.[15,16]

In an analogous manner, SiN_x and SiC_y thin films are successfully incorporated into active optical and optoelectronic devices due to their wide bandgap (2.3 eV for SiC_y and 5.1 eV for SiN_x), and elevated electrical breakdown voltage, including panel displays, lighting, and light-emitting devices.[4,17–19] In this respect, both types of Si-based coatings are employed as permeation barriers and encapsulation layers in light-emitting devices (LEDs), and organic LEDs (OLEDs),[20–23] as well as in the fabrication of various planar optical systems and optical waveguides.[24] Additionally, SiN_xC_y and SiN_x coatings are used or suggested as passivation layers in flexible electroluminescent devices.[25,26] It should also be noted that amorphous hydrogenated SiC_xO_z thin films are the subject of intense exploration as potential candidates for optoelectronic devices, due to their appealing photoluminescence characteristics. These include both white emission as well as emission in the blue at the highly desirable 1540 nm optical wavelength, when doped with erbium (Er).[27–30] Nitrogen-rich silicon and SiN_x films also serve as host matrix for Si nanocrystals for use in optoelectronic device applications.[31,32] Other applications include the use of hydrogenated amorphous silicon-nitrogen (a-SiN_x:H) films as an insulating layer in thin-film transistors

*Electrochemical Society Member.
[z]E-mail: executiveoffice@gelest.com

(TFT) for liquid-crystal display (LCD) and other emerging display systems.[15,16,33,34]

The application of SiN_x, SiC_y, and SiN_xC_y also extends into the green energy field,[15,16] primarily in solar cell applications. For example, microcrystalline and amorphous SiC_y coatings are employed as window layers in thin film solar cells.[35] And much like the case of the hard coatings and computer chip industries, SiN_x and SiC_y thin films are applied as passivation layers in silicon solar cells.[36,37] Other applications include the use of Si-rich SiN_x as host matrix for Si nanocrystals and Si nanoscale inclusions (Si-ni) light emitters for solar cell applications.[31,38] Likewise, SiN_x is witnessing extensive use in biotechnology and medical fields, especially in medical devices due to its high chemical stability, enhanced wear endurance, improved fracture toughness, and, unlike its carbide analog, elevated thermal shock resistance, and good biocompatibility.[39] The resulting functions include usages in medical devices similar to the applications described above for IC systems.

In addition, SiN_x can be employed as a protective coating in in vivo and in vitro environments, including, for example, viewing windows for medical devices, insulating membranes for cell electroporation, as well as in biosensors for a variety of health-related applications.[40] In vivo studies demonstrate that SiN_x can be considered biostable, although differences in bio-dissolution rates have been observed in films prepared by different deposition techniques.[32,41–43] The SiN_x materials are non-irritating. and are considered non-cytotoxic.[44] Furthermore, they are not substrates for bacterial colonization and do not inhibit osteogenesis.[45]

It is also worth noting that the mechanical, optical, and electronic characteristics of SiN_x and SiC_y can be tightly controlled and systematically customized as a function of carbon (C) and nitrogen (N) concentrations.[46,47] This feature makes the SiN_xC_y phase a prime candidate for applications which require micro-modulation of the SiN_xC_y system to enable adjustable properties, such as those requiring tunable optical bandgaps and refractive indicies. In particular, SiN_xC_y films were grown with a tunable bandgap in the range of 2.3eV to 5.0eV, depending on their C and N content.[48,49]

However, in most cases, the incorporation of other elements, particularly hydrogen, is not accounted for. It is more proper to designate amorphous hydrogenated silicon nitride as a-SiN_x:H. Not only does the amount of hydrogen incorporation affect physical, optical, and dielectric properties (in accordance with the Lorentz-Lorenz relationship)[50] in what is commonly referred to as SiN_x:H, the nature of the Si-H versus N-H bonding also plays a significant role in tailoring the resulting film characteristics.[46–49] Another influencing factor is the Pauling relative electronegativity of the Si, N, and H elements (namely, Si:1.90; N:3.04; H:2.20). Si-N and N-H bonds have relatively high dipole moments, while Si-H bonds have relatively low dipole moments. Thus, even if the atom % of film compositions prepared with different precursors are identical, the resulting films may have different atom bonding arrangements and the dielectric properties of the resulting films will vary.

Fundamental Properties of Silicon Nitride

A review of the state of the art in silicon nitride processing technologies must begin with a summary of the fundamental properties of known phases of silicon nitride. Unfortunately, the last fully comprehensive review of silicon nitride both in monolithic (bulk) and thin film forms predates current film deposition technologies.[51]

At present, there is no up-to-date compendium of single reference data that completely describes the properties of silicon nitride in all of its' forms and compositions. More recent articles have examined specific aspects of silicon nitride technologies.[52,53] In particular, the report by Riley[52] provides a historical review of the progress of the silicon nitride ceramic system, including its evolution into a variety of high grade ceramic materials. Corresponding properties such as crystal structure, lattice diffusion and defect chemistry, oxidation, production and general properties were assessed in detail. The work also surveyed the development of microstructure-properties functionality relationships. Also, the review by Hampshire[53] presented a survey of silicon nitride ceramics structure, processing, and properties, including microstructural development, sialons, and applications. Newer review articles of silicon nitride thin film deposition techniques are discussed in Overview of silicon nitride formation and deposition techniques section.

Silicon nitride with the nominal stoichiometry Si_3N_4 (c-Si_3N_4) occurs in three crystalline forms: α, β, and γ, while amorphous SiN_x (a-SiN_x) exists in various forms that display a range of physical, chemical, electrical, and mechanical properties. Additionally, the literature generally refers to crystalline and amorphous silicon nitride with different ratios of silicon to nitrogen as silicon nitride (namely, a-SiN_x, or c-SiN_x with $0 < x < 1.33$), although a few reports described significantly higher N/Si ratio.[25]

Table I presents nominal properties for silicon nitride. The data compilation should be considered as a guide by the reader for bulk or crystalline (c-SiN_x), polycrystalline (pc-SiN_x), amorphous non-hydrogenated (a-SiN_x) and hydrogenated (a- SiN_x:H) thin films. The data is intended to represent salient, but not absolute, properties of the various forms of SiN_x as determined at temperatures in the range of 20°–100°C, except for self-evident thermal properties. In this context, the data should provide a baseline in the review and analysis of the properties of SiN_x films as reported in the published work.

Overview of Silicon Nitride Formation and Deposition Techniques

In general, silicon nitride monolithic (bulk) and film structures can be prepared by: (1) solid phase synthesis (e.g., nitriding of Si, hot isostatic pressing of silicon nitride particles); (2) liquid phase synthesis (porous composite infiltration with thermal conversion or spin-on deposition with thermal conversion from liquid or polymeric precursors); and (3) vapor phase synthesis in primarily thin and ultrathin films.

Silicon nitride monolithic (bulk) growth methodologies.—Solid phase synthesis of silicon nitride is usually associated with structural ceramic synthesis and the huge literature in this area is often associated with aerospace and military applications,[53,54] but recently the technique has been extended to semiconductor substrates.[55]

Liquid phase synthesis, although it straddles application areas, is the least studied of the processes and less is known about the resulting film or bulk properties. Liquid phase synthesis, including spin-on and sol-gel techniques, is usually associated with linear (thermoplastic) polymers or crosslinked (thermoset) resins with alternating silicon and nitrogen atoms in their backbone, and are broadly denoted polysilazanes and aminosilanes.[56–60] Early work in this area was directed toward thermolytic or pyrolytic conversion of polysilazanes directly into shaped or structural silicon nitride ceramics.[61] The successful production of structural ceramics from liquid phase synthesis has not been achieved to date due to issues associated with ceramic yield, by-product diffusion, phase composition, density and chemical composition.

In terms of chemical composition one of the two major classes of polysilazanes, organopolysilazanes (structure 1), has organic carbon substitutions on the backbone leading in general to silicon carbonitrides.[62] Inorganic polysilazanes, alternately termed perhydridopolysilazanes (structure 2), lead more directly to silicon nitride structures, but the polymers themselves are apt to have stability issues that lead to variability in performance.

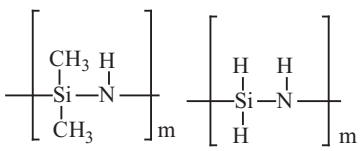

1 2

Table I. Overview of Properties of Bulk and Thin Film SiN_x*.

	Dense Bulk (crystalline/ polycrystalline)	Thin Films				
		a-SiN_x (H content <5%)			a-SiN_x:H (H content >5%)	
	c-Si_3N_4/pc-Si_3N_4	PVD	CVD	PECVD	CVD	PECVD
Physical						
Structure	Trigonal α-phase (Pearson symbol: hP28) or hexagonal β-phase (Pearson symbol: hP14)[52,53]	Amorphous				Amorphous
Density	3.19–3.20 g/cm^3 (Lube)[5] 3.1 g/cm^3 (Wang)[119]	Increased from 2.3 to 2.8 g/cm^3 with N/Si ratio from 0.0 to 1.1 (Schmidt)[120] Decreased from 1.97 to 1.82 with decreasing N/Si ratio from 1.42 to 1.15 (Serikawa)[121]	2.8 g/cm^3 (Joshi)[122]	2.6–3.0 g/cm^3 2.5 g/cm^3 (Hickernell)[123] 2.8 g/cm^3 for optimized film with N/Si ratio∼1.32 (Maeda)[124]	2.9 g/cm^3 (Carlotti)[125] 3.01 g/cm^3 (Joshi)[122]	2.5–2.8 g/cm^3 (Hickernell)[126] Increased from 2.62 to 2.90 g/cm^3 with Si/N ration from 1.04 to 1.53 (Taylor)[127] Varied from 2.0 to 2.7 g/cm^3 depending on preferential H bonding to Si or N (King)[128] Increased from ∼2.2 g/cm^3 for Si-rich films, with Si/N ∼ 1.1, to ∼2.4 g/cm^3 for N-rich films, Si/N∼0.5 (King)[129] 2.4 to 2.8 g/cm^3 depending on H content that ranged from 20 to 30% (Joshi)[122] Increased from 2.44 to 2.77 g/cm^3 with increasing N content for as-deposited films; Increased from 2.42 to 2.75 g/cm^3 with increasing N content for annealed films (Mei)[130]
Mechanical						
Hardness	9.0 Mohs	Increased from 15 to 28 GPa with N/Si ratio from 0.0 to 1.1 (Schmidt)[120] Increased from 9 to 23.4 GPa for as-deposited films with increased N/Ar flow in the sputtering chamber from ∼0.4 to no Ar (Vila)[131] Increased from 16.4 to 18.0 GPa for annealed films with increased annealing temperature from 1200 to 1350°C @100% N flow in the sputtering chamber (Vila)[131]	27.6 ± 2.0 GPa (Toivola)[132]			Increased from 16.1 to 19.8 GPa with Si/N ration from 1.04 to 1.53 (Taylor)[127] Varied from 13 to 23 GPa depending on preferential H bonding to Si or N (S. King 2010)[128] Increased from 2.62 to 2.90 g/cm^3 with Si/N ration from 1.04 to 1.53 (Taylor)[127]
Hardness, Knoop (100g)	2200 kg/mm^2 (Ferro-Ceramic)[133]					
Modulus of elasticity (Young's modulus)	320 GPa (Wang)[119]	Increased from 100 to 210 GPa As a function of deposition parameters (Vila)[131] Increased from 150 to 275 GPa with N/Si ratio from 0.0 to 1.1 (Schmidt)[120] Increased from 118 to 210 GPa for as-deposited films with increased N/Ar flow in the sputtering chamber from ∼0.4 to no Ar (Vila)[131] Increased from 174 to 183 GPa for annealed films with increased annealing temperature from 1200 to 1350°C @100% N flow in the sputtering chamber (Vila)[131]	222 ± 3 GPa (Vlassak)[134] Increased from 320–360 GPa with Si/N ratio from 0.83 to 0.95 (French)[135] 256 GPa (Carlotti)[125]	160GPa (Kramer)[136]	256 GPa (Carlotti)[125]	Increased from 178 to 221 GPa with Si/N ratio from 1.04 to 1.53 (Taylor)[127] Decreased from 420 GPa to 250 for N/Si ratio from 0.0 to 1.3, remaining constant above that ratio (Hasegawa)[137] Varied from 100 to 242 GPa depending on preferential H bonding to Si or N (King)[128] Decreased from 166.5 GPa for Si-rich films, with Si/N ∼ 1.1, to 64.5 GPa for N-rich films, Si/N∼0.5 (King)[129]
Tensile Strength	360–434 MPa (Ferro-Ceramic)[133]			2.4GPa (Ziebart)[138]		
Flexural Strength	400–950 MPa (Ziegler)[139]					
Compressive Strength	689–2760 MPa (Ferro-Ceramic)[133]					
Sheer Modulus	102–128 GPa					

Table I. ***Continued.***

	Dense Bulk (crystalline/ polycrystalline)	Thin Films				
		a-SiN_x (H content <5%)			a-SiN_x:H (H content >5%)	
	c-Si_3N_4/pc- Si_3N_4	PVD	CVD	PECVD	CVD	PECVD
Fracture toughness	5.8–8.5 MPa-m^{-2} (Ziegler)[139]					Decreased from 3.50 to 1.75 MPa-m^{-2} with increasing intrinsic film stress from −1200 MPa to 600 MPa for 2μm-thick films (King)[128] Remained constant ∼1.25 MPa-m^{-2} with increasing intrinsic film stress from −600 MPa to −50 MPa for 3μm-thick films (King)[128]
Poisson ratio	0.26 (Wang)[119]		0.28±0.05 (Vlassak)[134]	0.253 (Ziebart)[138]	0.28 (Carlotti)[125]	
Thermal						
Melting point	1900°C					
Thermal Expansion Coefficient	2.9 × 10^{-6} °C^{-1} (Wang)[119]				3.00 × 10^{-6}°C^{-1} (Carlotti)[125]	
Operating temp-continuous, max.	1000°C (Wang)[119]					
Operating temp-short-term, max.	1346°-1773° (Eckel)[140]					
CoE, × 10^{-6}	2.6–2.9 (Lube, Wang)[5,33]					
Heat Capacity, 20°–100°C	0.76 $Jg^{-1}K^{-1}$ (Lube)[5]		0.70 $Jg^{-1}K^{-1}$ (Mastrangelo)[141]			
Thermal transition, α-Si_3N_4 to -Si_3N_4	1400°–1500°C					
Thermal Conductivity	26 W/mK (Lube)[5]	1.2 W/mK (Govorokov)[142]	32 W/mK (Mastrangelo)[141] Intrinsic Thermal Conductivity increases from 2.0 W/mK to 2.5 W/mK with temperature increase from 70 to 200°C (Griffin)[143] Relatively flat @ ∼2.5–3.5 W/mK in the temperature range 77–350K (Sultan)[144]	Increased from ∼0.25 W/mK to ∼0.7 W/mk as temperature increased from 77 to 350K (Lee)[145] Increased from 0.8 to 1.7 W/mk as film thickness increased from 298nm to 1001nm (Bogner)[146]		
Thermal shock resistance	550–650°C/sec (NASA) 750°C/sec (Ferro-Ceramic)[133]					
Electrical						
Resistivity ρ	1 × 10^{-12}–10^{-13} ohm-cm	Decreased from 3 × 10^{13} to 3 × 10^{10} ohm-cm with decreasing N/Si ratio from 1.42 to 1.15 (Serikawa)[121] Si-rich and high O content exhibited ohmic behavior (ρ∼10^{10}−10^{11}ohm-cm); samples with high N/Si ratio and high oxygen showed space-charge limited-conduction behavior (ρ∼10^{12}−10^{13}ohm-cm); and stoichiometric samples with low oxygen content exhibited a Poole-Frankel conduction (ρ∼10^{11}−10^{13}ohm-cm) (Vila)[131]	10^{15} ohm-cm (Joshi)[122]	1 × 10^{-12} ohm-cm (Piccirillo)[147]	10^{17} ohm-cm (Joshi)[122]	<10^{15} ohm-cm (Joshi)[122]

Table I. ***Continued.***

	Dense Bulk (crystalline/ polycrystalline)	Thin Films				
		a-SiN_x (H content <5%)			a-SiN_x:H (H content >5%)	
	c-Si_3N_4/pc- Si_3N_4	PVD	CVD	PECVD	CVD	PECVD
	17.7 kV/mm (Ferro-Ceramic)[133]		10.0×10^6 V/cm (Joshi)[122]	Increased from 3.0 to ~4.9×10^6 V/cm for as deposited samples with increasing RF power density during deposition; Increased from ~2.2 to ~4.7×10^6 V/cm for annealed samples with increasing RF power density during deposition (Maeda)[124]	10.0×10^6 V/cm (Joshi)[122]	5.0×10^6 V/cm (Joshi)[122]
Dielectric Constant	1 MHz: 7.0–10.5 (Khan)[148]		6.0 (Joshi)[122]	7.0 (Piccirillo)[147] 6.31–7.56 (Maeda)[124]	7.0 (Joshi)[122]	6.0 to 9.0 depending on H content that ranged from 20 to 30% (Joshi)[122]
Optical						
Refractive Index	2.016 @ 589.3 nm 2.073 @ 400 nm	Decreased from 1.97 to 1.87 with decreasing N/Si ratio from 1.42 to 1.15 (Serikawa)[121] Increased from 1.6 to 1.73 with increased N flow ratio from 10 to 100% @1800nm (Signore)[149] Decreased from ~3.18 to ~2.01 with increasing N/Si ratio from 0.31 to 1.5 (Davis)[150]	2.07 2.01 (Joshi)[122]	Decreased from 2.19–2.07 @ 634nm with Si/N ratio from 0.83 to 0.95 (French)[135] Decreased from ~2.5 to ~2.1 with increasing N content (Davis)[150] 1.98 for optimized film with N/Si ratio~1.32 (Maeda)[124] Decreased from ~2.7 to ~1.6 with increasing N/Si ratio from 0 to 1.2 (Lowe)[151]	2.01 (Joshi)[122]	1.8–2.5 depending on increasing H content from 20 to 30% (Joshi)[122] Increased from 2.0–2.7 with higher N/Si ratio @350 nm (Charifi)[15 2] Increased from ~2.05 to ~2.12 with increasing deposition temperature from 300 to 500°C for as-deposited films; Increased from ~1.9 to ~2.07 with increasing deposition temperature from 300 to 500°C for annealed films (Mei)[130] Decreased from ~3.71 to ~2.03 with increasing N/Si ratio from 0.01 to 1.17 (Davis)[150]
Optical Gap			2.4–4.7			
Extinction Coefficient		Increased from ~0.03 to 0.65 with increased N flow ratio from 10 to 100% @200 nm (Signore)[149]	$<6 \times 10^{-4}$			Increased from 0.0–1.0 with higher N/Si ratio (Charifi)[152]
Tribological						
CoF, SiN mating, low speed	0.7 (Dante)[153]					
CoF, SiC mating, low speed	0.27 (Dante)[153]					
CoF, SiN mating, hydrodynamic, high speed	<0.002 (Dante)[153]					
Permeation/Absorption						
Water vapor transmission rate, 100 nm film			CVD: 7×10^{-3} g m^{-2}/day (Majee)[20] ALD: $2–5 \times 10^{-2}$ g m^{-2}/day (Carcia)[154]	0.015×10^{-2} gm^{-2}/day (Wuu)[155]		

*All values at R.T. unless otherwise indicated.

Limited commercial success of liquid phase synthesis has been the infiltration of porous ceramics followed by pyrolytic conversion to produce densified ceramic-matrix composites (CMCs),[63] as binders in metal-matrix composites (MMCs),[64] and as spin-on film for photolithography with materials supplied initially by Kion Corp and transitioned to Clariant and E Merck Corp.[65] Similarly, commercial acceptance was achieved in fabrication of dielectric layers by spin-on deposition techniques for semiconductor devices in a process in which silicon nitride initially formed from perhydridopolysilazane was ultimately converted to silicon dioxide[66,67] with materials supplied by Tonen Corp, but this approach has largely been abandoned.[68]

Silicon nitride thin film vapor processing technologies.—Silicon nitride thin film vapor processing technologies include physical vapor deposition (PVD), primarily sputtering; chemical vapor deposition (CVD) in its various forms, including thermal, hot wire (HW-CVD), plasma-enhanced (PE-CVD), and remote plasma-enhanced; and atomic layer deposition (ALD), also in thermal, plasma-assisted (PA-ALD), plasma-enhanced (PE-ALD), and remote plasma forms. In this context, Takeyama,[25] King,[11,12] and Meng,[13] present valuable historical reviews of silicon nitride PVD, CVD, and ALD deposition techniques.

PVD, which in principle involves the transport but not the formation of silicon nitride is an area of continued exploration since film composition and properties are influenced by sputtering methods as well as transport, and deposition environments.[69] There is emerging interest and reports of alternatives to ALD for ultra-thin films for both SiN_x and SiN_xC_y by self-limiting processes associated with self-assembled monolayer (SAM) deposition[70] and molecular layer deposition (MLD).[68,71,72]

Vapor phase synthesis is associated with the semiconductor, medical, aerospace, energy, and automotive sectors. As such, the present article will predominantly review the latest research work in vapor phase synthesis. In this respect, Tables II and III present details of very recent vapor phase deposition techniques of SiN_x thin films, along with a synopsis of intended applications.[15,16,20–25,31–34,36–38,73–101] More specifically, Table II summarizes PVD and CVD work, while Table III focuses exclusively on atomic layer deposition ALD.

It is worth noting that, historically, CVD in its various forms, including thermal, HW-CVD, PA-CVD, PE-CVD, and remote plasma-enhanced, had been the method of choice for growing SiN_x thin films, followed by PVD, mainly magnetron sputtering. More recently, however, ALD (including thermal, PA-ALD, and PE-ALD) appears to be receiving the most attention due to the need for extremely thin SiN_x films with increasingly tight control of composition and properties.

In what follows, an overview is first presented of silicon nitride source chemistries. In this context, Table IV outlines the Si- and N-bond dissociation energies for selected SiN_x source chemistries[102,103] while Table V focuses on relevant properties of many of the recently studied CVD and ALD SiN_x source precursors.[104] Subsequently, the various CVD, PVD, and ALD processes are summarized, respectively, in Appendices A, B, and C and discussed in more detail in the relevant sections.

Overview of Silicon Nitride Source Chemistries

It should be noted that in the case of CVD and ALD processes, the differences in formation and behavior of SiN_x thin films can be attributed, in part, to fundamental thermodynamic and chemical properties of precursors. In this context, Table IV lists bond dissociation energies for selected SiN_x source chemistries, not only those that are most commonly used, specifically, silane (SiH_4) and ammonia (NH_3). The table is intended to provide the reader with a baseline comparison of bond dissociation energies of selected organic and inorganic Si and N source chemistries with the most commonly used precursors, namely, silane (SiH_4) and ammonia (NH_3). Table V presents relevant properties of many of the recently studied CVD and ALD SiN_x source precursors. The precursors are divided into classes: perhydridosilanes, hydridohalosilanes, halosilanes and aminosilanes. Representative structures are depicted below.

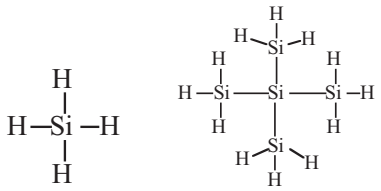

perhydridosilanes (silane, NPS)

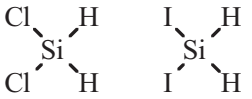

hydridohalosilanes (DCS, diiodosilane)

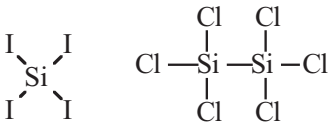

halosilanes (tetraiodosilane, HCDS)

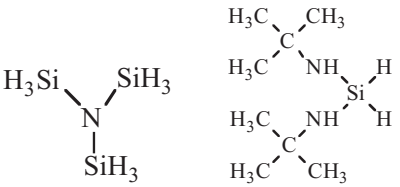

aminosilanes (TSA, BTBAS)

The large bond dissociation energy of N_2 and relatively high bond dissociation energy of SiH_4 are consistent with the fact that energetic environments, typically either thermal or plasma, are necessary for thin film formation. The resulting films tend to be rich in H and the H typically resides on the Si atoms, with post deposition thermal treatment commonly applied to reduce H content.[36,38,41,42] Since the N atom is trivalent and the silicon atom is tetravalent, H content in the film has minimal effect on the mobility of films: conformality is difficult to achieve and reflow is not observed in post-deposition process windows.[34,85,91]

In contrast, the lower dissociation energies associated with NH_3 and SiI_4 allows deposition at lower temperatures.[105,106] Additionally, chemical pathways associated with silicon diimide and diiodosilylene formation from SiI_4 are enabled for deposition. In this case, H mostly resides on the N atom on films formed from silicon halides and NH_3 with the important consequence that the mobility of H substituted N atoms are constrained in two dimensions rather than three. Conformality is therefore expected to be easier to achieve. This advantage is offset by the fact that the chemical deposition pathway leads to gas phase depletion reactions independent of the substrate.[73]

The discussion above is partly simplified, particularly in the case of CVD. Higher energy environments associated with CVD often induce gas phase depletion reactions initiated by unimolecular decomposition of a precursor and/or direct reaction of precursors in the gas phase preceding or concomitant with deposition.[107] ALD more often proceeds by direct reaction with surfaces or by a dissociative adsorption on surfaces (in rate limiting steps) and, as a result, associated reactions, by definition, proceed sequentially.[82,90]

Table II. Summary of Recent CVD, PECVD, and Sputtering SiN_x Work.

Deposition Technique	Potential Application	Brief Description	Reference
PE-CVD followed by patterning	Si solar cells	Passivation and dielectric layer	37
RF Magnetron Sputtering DC Magnetron Sputtering	Microelectromechanical systems (MEMS)	Barrier and passivation layers and etch stop.	74,116
PE-CVD and RF magnetron sputtering	Non-volatile memory (NVM) devices	Dielectric layer in stacked high-dielectric constant (κ) structures	75
RF PE-CVD (see also Reference 19)	Optical, electrical, and chemical devices	Overlays on cylindrical fused silica optical fibers	76
Hot Wire CVD	Organic electronic devices on polymer flexible substrates	Multilayers as permeation barriers	21
Surface-wave-plasma low temperature CVD	OLEDs	Highly water-impermeable transparent barrier and protective layer	22,23
Hot Wire CVD (HW-CVD) with post deposition Ar treatment	OLEDs and organic solar cells on polymer flexible substrates	Encapsulation and passivation layer	20
Remote-controlled Plasma-Enhanced CVD (PE-CVD)	Photoluminescent and optoelectronic devices, solar cells	Host for Si nanocrystals as active light emitters	32
Low-Pressure CVD with post-deposition thermal annealing	Non-volatile memory devices	Layer in metal–oxide–nitride-oxide–silicon semiconductor memory architectures	77
PE-CVD	Solar cells on graphite substrates	Passivation layer as part of a SiN_x/a-Si:H stack	78
RF Magnetron Sputtering and PE-CVD	Solar cells, through-Si vias for 3D devices, electroluminescent and display devices	Passivation and optical layer	25
Remote microwave PE-CVD	OLEDs	Anti-moisture permeation transparent barrier and protective layer	79
PECVD/RF PE-CVD	Organic Thin Film Transistors (TFTs)	Gate insulator	33
Low-Temperature Pulsed-RF PE-CVD	TFTs on fragile substrates, such as plastic or paper substrates	Gate and passivation dielectric, anti-reflective coating	34
PE-CVD with post-deposition rapid thermal annealing (RTA)	Photoluminescent and optoelectronic devices, solar cells	Host for Si nanocrystals as active light emitters	38
PE-CVD	Solar cells	Passivation layer	36
Radio-frequency (RF) PE-CVD (see also Reference 47)	Optical devices operating in the infrared spectral range (optical sensors, filters and resonators)	Optical layer in the infrared spectral range	24
Magnetron co-sputtering	Photoluminescent and optoelectronics devices	Si nanocrystals embedded in ultrathin SiN_x barrier layers	31
PE-CVD	Gallium Arsenide (GaAs) heterojunction bipolar transistors (HBTs)	Metal-insulator-metal (MIM) capacitor dielectric film	16

Chemical Vapor Deposition (CVD)

Appendix A presents a synopsis of SiN_x thermal, plasma-enhanced, hot-wire, and remote plasma-enhanced CVD parameters and post processing treatments (where applicable). Table II and Appendix A show the following common trends in recent CVD work:

- CVD SiN_x films are employed as barrier/protective layer, etch stop, and higher dielectric constant (κ) dielectric in IC microprocessor and memory (primarily metal-insulator-metal capacitor structures) devices;[75] transparent and, moisture permeation barriers, and dielectric layer in solar cells[32,37] and organic light-emitting devices (OLEDs).[22,23] More unique applications include SiN_x overlays on cylindrical fused silica optical fibers[76] and host material for Si nanocrystals as active light emitters,[38] both for use in photoluminescence (PL) and optoelectronics devices. One common attribute in all these applications is the inherent ability of CVD to provide conformal SiN_x coatings in complex topographical structures, such as high aspect ratio channels, vias, and trenches in IC applications.
- Silane (SiH_4) and ammonia (NH_3) are the predominant source chemistries for, respectively, silicon and nitrogen. Under PE-CVD conditions, high quality SiN_x films with minimal hydrogen content can be obtained in the temperature range of 300–400°C. This temperature range is also needed to yield higher density films with low porosity and surface roughness, since it allows longer surface diffusion length of adsorbed radicals in comparison to when lower substrate temperatures are applied.[31] Significantly lower substrate temperature (<100°C) was used in the case of polymer flexible and polyethyleneterephthalate substrates[20–23,79] to minimize thermal budget induced damage to the fragile plastics, resulting in a-SiN_x:H films with significant hydrogen content (>5%).[79] The inclusion of increasingly higher hydrogen content (up to 30%) with gradual decrease in processing temperatures was supported by other work.[25]
- CVD SiN_x thin film formation appears to involve the typical CVD reaction pathways:[108,109] (1) transport of gaseous SiH_4 and NH_3 precursor species to the substrate surface, in the case of thermal CVD, or the occurrence of gas phase reactions, in the case of PE-CVD or PA-CVD, followed by transport of the resulting gaseous reactants (e.g., SiH_x where $x < 4$ and NH_y where $y < 3$) to the surface; (2) adsorption of the Si-bearing and N-bearing species to substrate surface; (3) surface diffusion with potential desorption of some reactant groups; (4) surface reaction with film nucleation in island growth or step growth mode; and (5) emission of resulting volatile reaction products.[110] As mentioned above, higher substrate temperature allows longer surface diffusion lengths, leading to extended surface reaction times, and resulting in improved step coverage and reduced hydrogen incorporation. Alternatively, the pre-adsorption reactions in the case of PA-CVD or PE-CVD could produce more active reactant species, leading to higher surface reaction rates at shorter surface diffusion lengths, potentially producing less contaminated SiN_x films but with poorer step coverage and lower etch resistance.[107]
- Although a significant body of research in thermal CVD SiN_x can be found in the literature prior to 2010,[73,105,106,111–115] there are very few recent reports (within the last five years) on the topic, due most likely to the high thermal budget required for dissociation and reaction of the Si and N chemistries, except for

Table III. Summary of Recent ALD SiN_x Work.

Deposition Technique	Potential Application	Brief Description	Reference
Thermal ALD	Integrated Circuitry (IC) devices	Thin films in transistors, memory cells, logic devices, memory arrays	100
Plasma-Enhanced ALD (PE-ALD)	IC devices	Hydrofluoric acid (HF) etch stop layer and electrically insulating spacer	80
PE-ALD	IC, MEMS, and biomedical devices	HF etch stop layer and electrically insulating spacer	81
PE-ALD	MOSFET devices	Diffusion barrier	82
PE-ALD	IC devices	Gate spacer of dynamic random access memory and logic devices, and charge trap layer of 3D vertical NAND flash devices	83
PE-ALD	IC devices	Functional material for logic and memory devices	84
PE-ALD	IC logic and memory devices	Oxidation mask, diffusion barrier, gate dielectric, liner, and spacer	85
Thermal and Plasma-Assisted (PA-ALD)	IC logic and memory devices	Nitride spacer, floating gate	86
Thermal ALD	Non-volatile memory (NVM) devices	Dielectric layer in stacked high-κ structures	87
PA-ALD	IC devices, photovoltaic devices	Dielectric layer, sidewall spacer, hard etch mask, passivation layer, antireflection coating	88
PE-ALD	IC memory devices	Gate spacers for high κ transistors	92
PE-ALD	MOSFET devices	Spacer material	90
PE-ALD	Organic light-emitting diodes	Encapsulation layer against moisture and O_2 permeation	91
PE-ALD	IC devices	Barrier film and masking material	89
PE-ALD	IC logic and memory devices	High κ material, spacer material	93
PE-ALD	IC devices, photovoltaic devices	Anti-reflective coating, passivation and encapsulation layer, diffusion barriers, gate dielectric, stress liner	94
Thermal ALD	IC devices	passivation layer, barrier for alkali or moisture diffusion, masking layer, final protection layer	95
PE-ALD	IC devices	Liner and spacer material	96
Thermal or PE-ALD	IC devices	Spacer, mask	101
PE-ALD	IC devices	Spacer, etch stop material	11
PE-ALD	IC devices	Host matrix for Ru nanocrystals as seed/barrier layer for Cu metallization	97,98
Thermal ALD	IC devices	Dielectric material	117

noteworthy research on the thermal CVD reaction of dichlorosilane (SiH_2Cl_2) and nitrogen (N_2). This reaction required a substrate temperature of 750°C, which is prohibitively high for most electronic and solar applications.[77]

A significant report[34] included the use of pulsed RF generated by modulating a continuous 200Hz low-frequency wave signal generator with 50% duty cycle in the PE-CVD reaction of SiH_4 and NH_3 at 150°C. The process yielded film densification (over 20% increase in film density) and smoothing (a decrease in average surface grain size standard deviation from 0.2nm[2] to 0.04nm[2]), with the SiN_x films exhibiting smoother surface morphology and lower void density.

A common rule of thumb[32,38,75] in the PE-CVD and PA-CVD work appears to be that lower R = NH_3/SiH_4 flow ratios (R < 1) lead to Si-rich films (Si/N ratio > 1.1), while higher R (R > 1) produces N-rich films (N/Si ratio > 1.4), with inclusions of Si nanostructures or nanoscale intrusions at even higher R values. Also, lower substrate temperatures tend to yield a-SiN_x:H films, with thermal annealing required to reduce H content and lead to film crystallization, while higher processing temperatures produce c-SiN_x films with reduced hydrogen content. Comparable results were obtained in the case of PE-CVD SiN_x from a N_2+SiH_4 mixture, with Si-rich films being formed at higher N_2 flows.[75]

Studies of post-deposition thermal annealing effects were also reported under different annealing modes, gases, and durations, with[21] or without vacuum break between the deposition and annealing steps:[36,38,41,42]

In the case of in situ annealing,[21] SiN_x multilayered permeation barrier stacks deposited on PET substrates <100°C were transported to a PE-CVD chamber between every two successive 50-nm thick SiN_x layers and exposed to a 13.56 MHz RF Ar plasma at varying power density, working pressure, and treatment duration. The work led to the identification of an optimized Ar plasma treatment

Table IV. Si- and N- Bond Dissociation Energies for Selected SiN_x Source Chemistries*.

Source Precursor		Bond Dissociation Energy (kJ/mole)
Nitrogen		
	N_2 (N-N)	946
	NH_3 (N-H)	435
	H_2NNH_2 (N –N)	272
Silicon		
	$SiCl_4$ (Si-Cl)	460
	H_3SiCl (Si-Cl)	456
	$HSiCl_3$ (Si-H)	394
	SiH_4 (Si-H)	384
	$SiBr_4$ (Si-Br)	377
	Si_2H_6 (Si-H)	374
	Si_2H_6 (Si-Si)	321
	SiI_4 (Si-I)	284

*The table is intended to provide baseline comparisons of bond dissociation energies of selected organic and inorganic Si and N source chemistries with the most commonly used precursors.[102,103]

Table V. Relevant Properties of Recently Studied CVD and ALD SiN_x Source Precursors.

Class	Name	Acronym	Formula	Molecular Weight	% Si	form	Boiling Point	Melting Point	Vapor Pressure	Density
							°C	°C	°C: torr	g/cm^{-3}
Perhydridosilanes										
	silane		SiH_4	32.12	87.4	gas	−112°	−185°	−110°:775	0.680
	disilane		Si_2H_6	62.22	90.3	gas	−14.5°	−132°	21.1°:2586	0.686
	trisilane		Si_3H_8	92.32	91.2	liquid	52.9°	−117°	0°: 95.5	0.743
	n-tetrasilane		Si_4H_{10}	122.42	91.7	liquid	106°	−85 to −95°	20°: 22	0.825
	isotetrasilane		Si_4H_{10}	122.42	91.7	liquid	101°	−99°	20°: 25	0.793
	neopentasilane	NPS	Si_5H_{12}	152.52	92.1	liquid	132–134°	<−40°	25°:15	0.805
Hydridohalosilanes										
	monochlororosilane	MCS	SiH_3Cl	66.56	42.2	gas	−30.4°	118°	25°: 4900	1.145
	dichlorosilane	DCS	SiH_2Cl_2	101.01	27.8	gas	8.3°	−122°	−34°: 100	1.22
	diiodosilane	DIS	SiH_2I_2	283.91	9.9	liquid	149−150°	−1°	55°:25	2.834
	triiodosilane		$SiHI_3$	409.81	31.0	liquid	220°	8°	95°: 12	3.314
Halosilanes										
	tetrachlorosilane		$SiCl_4$	169.90	16.5	liquid	57.6°	−70°	20°: 194	1.481
	hexachlorodisilane	HCDS	Si_2Cl_6	268.89	20.9	liquid	144−6°	−1°	85°: 109	1.562
	octachlorotrisilane	OCTS	Si_3Cl_8	367.88	22.9	liquid	213–5°	−67°	90°:10	1.61
	tetrabromosilane		$SiBr_4$	347.70	8.1	liquid	154°	5°	0°:1.8	2.772
	tetraiodosilane		SiI_4	535.70	5.2	solid	287–8°	120–1°	125°:∼30	4.198
Aminosilanes										
	trisilylamine	TSA	Si_3H_9N	107.33	78.5	liquid	52°	−106°	0°: 110	0.895
	bis(diethylamino)silane	BDEAS	$SiH_{22}C_8N_2$	174.36	16.1	liquid	188–189°	<0°	70°:30	0.804
	bis(t-butylamino)silane	BTBAS	$SiH_{22}C_8N_2$	174.36	16.1	liquid	167°	<−50°	25°: 1.15	0.816
	tris(dimethylamino)silane	3DMAS	$SiCH_{19}C_6N_3$	161.32	17.4	liquid	145–8°	−90°	4°: 16	0.838
	tris(isopropylamino)silane	TIPAS	$SiH_{25}C_9N_3$	203.40	13.8	liquid	165–166°		25°: 1	
	tetrakis(ethylamino)silane	TEAS	$SiH_{24}C_8N_4$	204.39	13.7	liquid	>90°-dec.	<0°	25°: 1.3	
	tetrakis(dimethylamino)silane	4DMAS	$SiH_{24}C_8N_4$	204.39	13.7	liquid	180°	−2°	75°: 19	0.885
	bis(dimethylaminomethylsilyl)-trimethylsilylamine	DTDN-2H$_2$	$Si_3C_9H_{29}N_3$	263.60	32.0	liquid	237°		60°: 1.0	
	tris(isopropyl)cyclotrisilazane	TICTZ	$Si_3C_9H_{27}N_3$	261.59	32.2	liquid	220–224°	−69° to −71°	67°: 1.8	0.919
	tetramethyldisilazane	TMDZ	$Si_2C_4H_{15}N$	133.34	42.1	liquid	99–100°	<−60°	25°: 55	0.766
	diisopropylaminosilane	DIPAS	$SiC_6H_{17}N$	131.30	21.4	liquid	117°	<−20°	55°: 106	0.76

Data in this table from sources cited in text or experimentally determined by the authors.

recipe for the formation of improved permeation barriers, with the finding being attributed to the role of Ar plasma in rearranging Si and N atoms at the SiN_x layers interfaces, thus causing a densification of the interfacial regions, and an ensuing reduction in the permeability of the SiN_x multilayered stacks.

In the case of annealing in a conventional oven with vacuum break, one study[41,42] performed annealing of Si-rich SiN_x films in a conventional oven in N_2 flow, with thermal treatment at 1100°C leading to the formation of Si nanocrystals (Si-NCs) within the SiN_x host matrix. The Si-NCs acted to significantly enhance the SiN_x films photoluminescence properties due to quantum confinement effects. In another study,[36] SiN_x samples were annealed in a conventional oven at 830°C to improve hydrogen passivation and ensure reduced leakage current in the resulting metal-insulator-semiconductor (MIS) structures.

Alternatively, another approach[38] implemented rapid thermal annealing (RTA) with vacuum break in pure Ar, Ar with 20% O_2, and Ar with 50% O_2 of Si nanoscale intrusions (Si-ni) embedded in Si-rich SiN_x films. It was found that only at temperatures above 950°C did the thermal treatment have any effect on the optical properties of the Si nanoscale intrusions, although the effect was less significant than the NH_3 to SiH_4 ratio during the deposition step.

Physical Vapor Deposition (PVD)

Appendix B presents a synopsis of SiN_x sputtering parameters and post processing treatments (where applicable). A review of Table II and Appendix B shows the following common trends in recent sputtering work:

Most common applications for sputtered SiN_x films consist primarily of a barrier/passivation coating and etch stop in microelectromechanical systems (MEMS);[74,116] high refractive index material for solar cells,[25] through-Si vias for three-dimensional (3D) semiconductor devices, electroluminescent devices, and display devices;[25,31] and high κ dielectric layer in stacked high-dielectric constant (κ) structures for non-volatile memory (NVM) devices.[75] A unique application is as a host material for Si nanocrystals as active light emitters for uses in PL and optoelectronic devices. Given that sputtering tends to be a line of sight technique, the application of sputtering techniques is primarily limited to topographies that are less aggressive with more relaxed design rules and smaller aspect ratios than their CVD and ALD counterparts.

DC or RF magnetron sputtering were the deposition techniques of choice for PVD, although the deposition rates for RF magnetron sputtered SiN_x were significantly lower than their DC counterparts.[74,116] Furthermore, the DC magnetron sputtered SiN_x films exhibited superior chemical and physical properties than their RF magnetron sputtered analogs, while displaying equivalent electrical characteristics in MEMS devices.

These findings support the conclusion that DC magnetron sputtered films are more suitable than their RF equivalents for most SiN_x applications, except in cases where substrates are mechanically or chemically fragile, thus requiring reduced impact energy to minimize ion and radical Induced damage.

In DC magnetron sputter work,[116] it was shown that the N_2 plasma back pressure played a key role in modulating the N/Si ratio in the resulting SiN_x films, with higher back pressures leading to increased N content in the films. Alternatively, in another report, the N/Si ratio in SiN_x films was controlled by employing RF Magnetron sputtering to produce Si-rich films, and PE-CVD to yield N-rich films.[74]

A pertinent report[25] compared the properties of SiN_x films grown by RF magnetron sputtering and PE-CVD at low temperature. The resulting findings indicated that sputtering was more appropriate than PE-CVD in yielding higher quality SiN_x films with enhanced density, with the lower density in the PE-CVD coatings being attributed to the inclusion of hydrogen (due to the lower processing temperature employed).[25]

Another report of note[31] focused on the formation of Si nanocrystals (Si-NC) in multilayered structures consisting of alternating Si-rich SiN_x (SRN) and Si_3N_4 ultrathin films. In this case, the N/Si ratio in the SRN layers was regulated by co-sputtering from Si (DC magnetron sputtering) and Si_3N_4 (RF magnetron sputtering) targets. The Si content in the resulting SRN films was modulated by adjusting the deposition rates from the targets through control of the power applied to the targets, with the application of higher DC power to the Si target leading to an increase in Si concentration. Alternatively, stoichiometric Si_3N_4 ultrathin films were achieved by RF magnetron sputtering from the stoichiometric target. After the formation of 25 alternating layers consisting of 5 nm thick SRN and 1nm thick Si_3N_4, the structures were capped with a 10 nm-thick Si_3N_4 protective coating and annealed above 900°C in N_2 environment to form Si-NCs in the Si-rich layers. The annealing step led to improved PL performance, which was attributed to improved crystallization and enhanced nitride passivation in the Si-rich layers.

Atomic Layer Deposition (ALD)

Appendix C presents a synopsis of SiN_x thermal, plasma-assisted, and plasma-enhanced ALD parameters and post processing treatments (where applicable). A simple first-order observation is that under similar conditions, regardless of technique, growth per cycle (GPC) is significantly greater with precursors containing multiple silicon atoms. For example, neopentasilane has a higher growth rate than silane. Similarly, hexachlorodisilane has a higher growth rate than dichlorosilane.[113] Table III and Appendix C reveal the following additional trends in recent ALD work:

The most common applications for ALD SiN_x films are barrier/protective layer, etch stop, passivation layer, spacer material, and high dielectric constant (κ) dielectric in emerging nanoscale IC microprocessor and memory devices[100] and, to a lesser extent, transparent barrier, anti-reflective coating, anti-moisture permeation layer, and dielectric layer in solar cell and OLED systems.[88] Other applications include host matrix for ruthenium nanocrystals as seed/barrier layer for copper metallization in IC structures;[97,98] and hydrofluoric acid etch stop layer and electrically insulating spacer in MEMS and medical devices.[80,81] One common attribute in all these applications is the inherent ability of ALD to provide stringent atomic level control and excellent conformality[55] for SiN_x coatings in challenging geometries where CVD begins to show its deficiencies and shortcomings. These geometries include highly complex topographical structures, such as extremely high aspect ratio or exceedingly narrow channels, vias, and trenches in IC applications.

In contrast to recent CVD work, very few ALD reports used SiH_4 and other perhydridosilanes, such as neopentasilane ($(SiH_3)_4Si$), as Si source chemistry.[11,85] Instead, the Si sources employed in the most recent ALD investigations could be organized into two categories: (a) inorganic Si sources, including hydridosilanes, such as monochlorosilane (SiH_3Cl),[93] dichlorosilane (SiH_2Cl_2),[93] and diiodosilane (SiH_2I_2);[101] and halosilanes, such as hexachlorodisilane (Si_2Cl_6),[82,88,117] Octachlorotrisilane (Si_3Cl_8),[87] and tetraiodosilane (SiI_4);[86,100,101] and (b) organic Si sources, primarily amidosilanes, such as BTBAS ($SiN_2C_8H_{22}$).[92,93] For nitrogen, the majority of the work described the use of NH_3 or N_2. One report suggested the additional use of hydrazine (N_2H_4),[101] which is quite undesirable given its elevated toxicity and high instability, while another proposed the utilization of t-butylhydrazine ($C_4H_{12}N_2$).[100] Although no dissociation energy is available in the literature for t-butylhydrazine, it is estimated to be significantly lower than N_2 based on reports in the literature on the dissociation energy of N_2H_2,[103] thus making t-butylhydrazine more conducive for ALD growth of SiN_x at lower temperatures than N_2.

ALD SiN_x work[86,87,100,117] was carried out in three different modes: thermal (no plasma), PA-ALD (where the plasma was generated in the reactor directly above the substrate), and PE-ALD (where the plasma was generated remotely and transported into the reactor).

For thermal ALD, the majority of the work focused on the reaction of halosilanes and N-bearing reactants, including: (a) SiI_4 and NH_3 or $C_4H_{12}N_2$ in the temperature range of 175–250°C;[100] (b) Si halides containing Br and/or I (e.g., SiI_4, $SiBr_4$, $SiBr_{4-x}I_x$ ($x = 1–3$), or Si_yX_{2y+2}, where $y > 2$, and X is one or more Br or I) and a N-containing reactant, such as NH_3, in the temperature range of 350–600°C;[86] (c) Si_3Cl_8 and NH_3 in the temperature range of 310–500°C;[87] (d) Si_2Cl_6 and NH_3 in the temperature range of 515–573°C.[117] Only two of the reports[87,117] presented compositional analysis results for the SiN_x films. The findings indicated that lower deposition temperatures produced sub-stoichiometric films that oxidized upon exposure to air. Higher processing temperatures generated films that were closer to a N/Si ratio of ~1.3, and led to a reduction but not complete elimination of oxidation upon removal from the ALD reactor. These results suggest that thermal ALD might require prohibitively higher deposition temperatures (well above 573°C) to yield stoichiometric films with effective resistance to oxidation.

PA-ALD SiN_x is the subject of relatively few reports,[86,88] and the work focused on the reaction of halosilanes and N-bearing reactants, primarily: (a) Si halides containing Br and/or I (See section Overview of silicon nitride source chemistries) and a N-containing reactant, such as NH_3, in the temperature range of 350–600°C;[86] and (b) Si_2Cl_6 and NH_3 in the temperature range 350–450°C.[88] The apparent lack of interest in PA-ALD SiN_x could be attributed, at least in part, to concerns about the potential adverse effects of plasma generation directly above the substrate, including the potential inclusion of contaminants in the films. Furthermore, compositional analysis[88] showed that the PA-ALD films were N-rich (N/Si ratio ~1.71) with significant H incorporation (e.g., as high as 23% at 400°C). Infrared studies[88] supported the preferential reaction of Si_2Cl_6 with surface NH_2 clusters, instead of NH groups, with the latter being incorporated in the SiN_x films due to their reduced reactivity with Si_2Cl_6. Interestingly, the infrared analysis demonstrated that the inclusion of H in the films was primarily in the form of NH species. This is consistent with earlier reports of Atmospheric Pressure CVD (APCVD) silicon nitride generated from iodosilanes.[105,106]

Most recent ALD work consisted of plasma assisted processing, wherein the plasma was generated remotely and transported into the reactor.[11,79–85,89–94,96–98,100,101,117] The benefits of remote plasma include lower deposition temperatures while ensuring minimal plasma-induced damage, exclusion of

undesirable gas-phase reactions, and reduction in surface nucleation time. As mentioned above, the Si sources employed in PE-ALD investigations could be organized into two categories: (a) inorganic Si sources, including perhydridosilane, hydridosilanes and halosilanes and (b) organic Si sources, primarily amidosilanes.

A number of reports examined the role of substrate temperature in PE-ALD SiN_x, with primary focus on the effects of low thermal budget on PE-ALD process characteristics and resulting film composition and chemical and electrical properties. One such report investigated low temperature PE-ALD growth from bis(t-butylamino)silane (BTBAS) and a N_2+Ar plasma at 150°C.[91] Subsequent structural and chemical characterization of the SiN_x layers indicated the absence of open pores larger than 0.3nm in diameter, with films as thin as 10 nm displaying good barrier properties. A second investigation examined low temperature PE-ALD (<300°C)[85] of SiN_x films from neopentasilane (NPS) as source chemistry using trisilylamine (TSA) as comparative baseline. The study determined that both precursors exhibited similar N_2 plasma saturation behavior, with NPS displaying higher growth rates. The films were Si rich (Si/N ratio ∼1.13) with minimal O and C contaminants. A third study[94] analyzed the thermal dependence of PE-ALD SiN_x films grown from trisilylamine (TSA) and NH_3 in the temperature range 250–350°C. All the films were nearly stoichiometric (N/Si ratio increased from 1.32 at 250°C to 1.35 at 350°C). Alternatively, hydrogen content decreased from ∼13% to ∼8% with the rise in thermal budget. In terms of higher temperature growth, processing temperatures of 400°C and 500°C were used in the PE-ALD of SiN_x from NH_3 and, respectively, monochlorosilane (MCS) and dichlorosilane (DCS).[93] The work demonstrated that the resulting SiN_x spacer (grown at 400°C) and gate encapsulation (deposited at 500°C) were crucial components in successful high-κ metal gate applications. Similar findings were presented[100] for PE-ALD SiN_x from Si precursors containing an iodine ligand (such as $HSiI_3$, H_2SiI_2, or H_3SiI) and a N-containing plasma. The resulting N/Si ratio ranged from 0.5 to 2.0. The findings are consistent with prior work that employed tetraiodosilane and titanium tetraiodide to generate Ti-Si-N diffusion barriers for copper metallization at low temperatures.[73]

In terms of the PE-ALD adsorption and decomposition mechanisms for inorganic sources, one relevant report[82] analyzed the reactivity of β-Si_3N_4 surface sites with Si_2Cl_6 (using SiH_4 as comparative baseline) during the PE-ALD Si_2Cl_6 substrate exposure step by combining ab initio density functional theory calculations with actual PE-ALD SiN_x film deposition. The analysis examined three types of substrate surface sites: (a) hydrogen passivated N and Si sites (NH/SiH); (b) NH and $SiNH_2$ sites formed during the NH_3 exposure step (NH/$SiNH_2$); and (c) under-coordinated bare Si=N sites. It was determined that the bare Si=N sites were more energetically favorable than their NH/SiH and NH/$SiNH_2$ counterparts to react with the Si or Cl atoms from the source precursors. It was also concluded that the reaction energy was lower for Si_2Cl_6 than SiH_4. These findings led to the identification of a 3 step PE-ALD process to attain the most energetically favorable surface sites during the Si source PE-ALD substrate exposure step.[82] Another investigation[11] also explored the role of a N_2 plasma pre-treatment prior to the SiH_4 exposure step on Si substrates and found that atomic N and N^+ are the central reactant species that adsorb to the Si surface to form Si-N. The latter then act as reactive adsorption spots for SiH_4 at N dangling bond sites, generating adsorbed SiH_x and NH_x species. Further adsorption is excluded until subsequent exposure to the N_2 plasma, leading to a repetition of the previous N species adsorption cycle. Reiterating the alternating N_2 plasma/SiH_4 exposure steps results in the growth of a complete Si-N layer followed by the formation of a continuous SiN_x film. This alternating exposure process was applied to produce SiN_x:H films with enhanced conformality and improved moisture barrier behavior.

In terms of the PE-ALD adsorption and decomposition mechanisms for organic sources, a similar theoretical and experimental study[82] of the energies of adsorption and decomposition of bis(dimethylaminomethylsilyl)trimethylsilylamine (DTDN2-H2, $C_9H_{29}N_3Si_3$) during DTDN2-H2 exposure step on the growing PE-ALD SiN_x film surface. The bare Si=N sites (as formed by the N_2 plasma) were found to be the most energetically favorable for the adsorption and reaction of DTDN2-H2. The study also showed that the N/Si ratio in the films increased from 0.98 to 0.99 as the substrate temperature was raised from 300°C to 400°C, with oxygen content ∼7.5% due to oxidation upon exposure to air. Further increase in substrate temperature to 500°C caused higher C incorporation, as well as a significant increase in O content. Alternatively, another study[90] combined first-principles density functional theory with experimentation to examine the effects of N-bearing plasmas (N_2, H_2, N_2-H_2, NH_3) on the mechanisms of adsorption of bis(t-butylamino)silane (BTBAS, $SiN_2C_8H_{31}$) on β-Si_3N_4 (0001) surfaces with various surface terminations. The study concluded that the use of H_2, N_2-H_2, and NH_3 plasmas caused termination of reactive β-Si_3N_4 (0001) surface sites with H and NH_x species, thus inhibiting precursor adsorption and film formation. The study also determined that the application of a N_2 plasma did regenerate reactive surface sites terminated with H and NH_2 groups. Interestingly, a complementary investigation[92] for PE-ALD SiN_x from BTBAS pointed to the existence of so-called "redeposition effects" resulting from the dissociation of reaction species in the plasma and the redeposition of fragments of such species on the surface of the growing SiN_x film. It was found that this effect is driven primarily by the plasma gas residence time, with a shorter residence time leading to a reduction in re-deposition effects and yielding films of higher purity and improved quality.

A report of note[96] incorporated ab initio techniques into theoretical models to examine the effects of PE-ALD reaction mechanisms on precursor adsorption and decomposition pathways for a variety of inorganic and organic Si precursors, including SiH_4, SiH_2Cl_2, $SiH_2(CH_3)_2$, $(Si_3N_4)_4(NH_3)_{12}$, and $SiN_2C_8H_{22}$. The techniques employed realistic cluster models of amine-covered surfaces to derive the configurations and energies of chemisorption and reaction of these Si sources via functional groups removal. These calculations were combined with density functional theory derivations that determined that the initial precursor physisorption phase was essential toward SiN_x film formation, which led to accurate predictions regarding the reactivity of a collection of amino-silane precursors. The theoretical derivations also provided correct projections on H retention in the PE-ALD SiN_x films. A recent report used density functional theory to model the dissociative chemisorption of silicon nitride precursors (mono(alkylamino)silanes) on silicon dioxide to determine the effect of different aminoalkyl ligands.[118] Adsorption energies, driven primarily by hydrogen bonding did not vary significantly with size of aminoalkyl ligands, however, a large variation in the reaction energy barriers was observed with ligand size due to transition state interactions and steric effects. The ALD window for suitable thin film growth was found to be widest for diisopropylaminosilane (DIPAS) and dipropylaminosilane (DPAS) precursors (∼100°C–500°C).

Another report[97,98] of note developed a PE-ALD SiN_x process as part of forming $RuSiN_x$ films as diffusion barriers for copper (Cu) interconnects for IC applications. The process employed tris(isopropylamino)silane (TIPAS) and NH_3 for SiN_x. $RuSiN_x$ films with varying Ru/SiN_x ratios were formed by controlling the number of PE-ALD SiN_x formation cycles while maintaining that for PE-ALD Ru constant. The resulting $RuSiN_x$ ternary phase consisted of an amorphous SiN_x host matrix con-

taining Ru nanoclusters of ∼3 nm in diameter, and exhibited stable diffusion barrier performance against Cu diffusion up to 650°C.

Studies of pre-, during, and post-deposition plasma treatment effects were also reported under different treatment modes, gases, and durations, with and without vacuum break between the deposition and treatment steps. Some of the key findings are reported below:

In the case of pre-deposition plasma treatment, substrate exposure to Ar plasma prior to SiN_x thermal ALD was shown to yield significantly lower SiN_x wet etch rates (WERs) compared to the case of no plasma treatment.[86] Alternatively, the opposite effect was observed in the case of a post-deposition H_2 plasma treatment,[81] which was attributed to the role of H_2 plasma in removing contaminants from the film or causing its densification. A similar finding was reported in the post-deposition treatment in a H_2 plasma for 3 hours at 350°C, which was ascribed to the efficacy of the H_2 plasma at residual C removal from the films.

Ar plasma was also observed to improve surface adsorption and activation pathways for PE-ALD SiN_x from DIPAS and NH_3.[84] In this work, successful SiN_x low temperature chemisorption (325°C) was achieved through the application of an additional Ar plasma treatment step after the Si precursor purge step, but prior to the NH_3 exposure cycle. However, when the intermediate number of Ar plasma treatments was increased from 1 to 3, the resulting films exhibited a rise in C and O contamination from, respectively, 0 to 10% and ∼15 to 30%. The films were Si rich with Si/N ratio over 2.

Alternatively, in PE-ALD of SiN_x from BTBAS and N_2,[92] it was shown that a constant increase in N_2 plasma exposure time led to a continuous decrease in C content at lower deposition temperatures (<500°C). For example, for films grown at 200°C, C content decreased from ∼15% at 1s N_2 plasma exposure time to ∼8% at 15s N_2 plasma exposure time. Films formed at N_2 plasma exposure times below 15s showed high affinity to O, while those deposited at 15s exhibited good resistance to oxidation. However, the composition of SiN_x films grown at 500°C was nearly stoichiometric (Si_3N_4), with minimal O and C contents, irrespective of N_2 plasma exposure time.

Summary and Commentary

The authors have presented an overview of the most recent published work (last five years or so) for SiN_x and SiN_x-rich films, primarily SiN_x with C inclusion, $SiN_x(C)$. This survey highlights major emerging developments in the SiN_x material system technologies, with focus on Si and N source chemistries and thin film deposition processes and their effects on resulting properties. It also demonstrates that SiN_x is the subject of an ever-growing interest and that its use is expanding into new technological areas.

From a chemistry perspective, and while generalizations are difficult when such a wide range of SiN_x applications is considered, certain trends are observed. Traditionally, SiN_x deposition, particularly in IC devices, utilized Si- and N-rich precursors such as SiH_4 and N_2 in relatively high-energy environments (>700°C or the use of plasma activation to achieve deposition at lower substrate temperatures). More recently, there has been a continual push toward lower energy deposition processes (reduced processing temperature) driven by the need to minimize thermal budget induced damage to thermally fragile substrates, such as low dielectric constant (κ) materials in IC devices and polymer materials in OLED applications. This need has engendered the utilization of precursors that possess "pre-assembled" Si-N bonds as exemplified by "single-source" precursors such as trisilylamine and, in order to achieve deposition in even lower energy environments, precursors that contain C, such as bis(t-butylamino)silane. Concomitant with this trend, there was recognition that desirable dielectric or passivation properties could be achieved despite the adventitious incorporation of C into films. Functional or performance properties, independent of a simple compositional definition of SiN_x, expanded interest in reproducible film formation with controlled and reproducible C inclusion. Silicon carbonitride films became widely accepted and deposition techniques and conditions were explored. As dimension constraints became tighter and ALD techniques became generally accepted, the differences in gas-phase and substrate reactivity with Si-N, Si-C, C-N and Si-halide bonds have been exploited and furthered the evolution and introduction of new precursors.

Another independent trend that is readily recognized is the acceptance of silicon halides as precursors. Historically, while silicon halides react with ammonia and other amines at low temperature, thus making them attractive for lower energy deposition processes, the low gravimetric percentage of silicon in precursors and the troublesome ammonium salt byproducts would have eliminated them from consideration. The acceptance of hexachlorodisilane as a SiN_x precursor in full-scale manufacturing is leading to consideration of other silicon halides such as tetraiodosilane in near-term full-scale manufacturing. Inherent in the development of SiN_x films is the evolution of SiN_x as an encompassing descriptor of the technology to Si-N rich films, such as SiN_x with C inclusion, $SiN_x(C)$, as well as the precursors and the deposition techniques used to achieve these films.

From a processing perspective, CVD in its various forms, including thermal, hot wire (HW-CVD), plasma-enhanced (PE-CVD), and remote plasma-enhanced CVD, had been historically the method of choice for growing SiN_x thin films, followed by physical vapor deposition (PVD), primarily magnetron sputtering. More recently, however, ALD has been receiving the most attention due to the need for extremely thin SiN_x films with tight control in composition and properties. This trend is attributed to the inherent ability of ALD to provide strict atomic level control and excellent conformality for SiN_x thin films in aggressive geometries where CVD begins to suffer from poor step coverage. These geometries include highly complex topographical structures, such as extremely high aspect ratio or exceedingly narrow channels, vias, and trenches in IC applications.

Another trend that has contributed to the growth of interest in Si-N rich films is the area of heterodevices. Until now, the primary driver for thin film materials has been the manufacture of IC devices. Despite the enormous scholarly literature in virtually every area of thin film technology for microelectronics, there has been little opportunity for new techniques to achieve adoption in full-scale IC manufacturing. Heterodevices, particularly those associated with life sciences, have different sets of material requirements and can be successful at lower manufacturing scale. Heterodevices open a wide range of new commercialization opportunities for silicon nitrogen-rich materials. The field of Si-N rich films will continue to evolve with new film requirements, new techniques such as Molecular Layer Deposition (MLD) and Self-Assembled Monolayers (SAMs) and associated new Si- and N- precursors.

Acknowledgments

The authors thank Sean King for his invaluable input and helpful discussions.

Appendix A. Summary of SiN_x Thermal, Plasma-Enhanced, Hot-Wire, and Remote Plasma-Enhanced Chemical Vapor Phase Deposition Parameters and Post Processing Treatments.

Reactor Type	Subs. Type	Subs. T (°C)	NH_3 Flow Rate (sccm)	SiH_4 Flow Rate (sccm)	H_2 Flow Rate (sccm)	Duration of Deposit. (sec)	Working Pressure (torr)	RF Power (W) or Power Density (W/cm^2)	Film Thick. (nm)	Post Deposition Treatment	Pertinent Details	Reference
Standard PE-CVD chamber	(100) p-type boron-doped monocrystal. Si substrates (ρ = 1–3 Ωcm)	350	N/A R = SiH_4/NH_3 flow ratio = 1		None	N/A	3.5	0.75	80	None reported	The intent of the work is to demonstrate a strategy for the indirect removal of SiN_x by patterning an a-Si:H etch mask with an 800 nm 140 fs laser	37
Standard PE-CVD chamber	4.5 nm to 7 nm-thick HfO_2 films	350	N/A	N/A	N/A	N/A	N/A	1000 W	12	None Reported	The PE-CVD SiN_x films were deposited on 4.5 nm to 7 nm-thick HfO_2 with x = 1.33 (N-rich SiN_x)	75
Standard PE-CVD chamber	(100) p-type Si subs (ρ = 1–10 Ωcm) Cylindrical fused silica optical fibers (length from 2.5–8mm and diameters of 125 μm and 400 μm)	200	50	150	None	900	~0.9	50 W	80	None reported	Investigation of the influence of optical fibers' suspension height and diameter on SiN_x deposition rate and resulting properties	76
HW-CVD reactor with single coil shaped hot Ta filament as catalyst to decompose reactants (SiH_4 and NH_3 diluted in H_2) Filament placed at 7.5 cm to minimize its effect on substrate temperature	175 μm-thick plastic substrates (heat stabilized PET with a stiffness of 3×10^{-3} N.m planarized on one side	<100	N/A	N/A	N/A	N/A	N/A	N/A	45–50 per SiN_x layer	Samples transported without vacuum break to a PE-CVD chamber for Ar plasma treatment @13.56 MHz and 350 mW/cm^2 in-between deposition steps	Permeation barriers for organic electronic devices on polymer flexible substrates were realized by combining stacked silicon nitride (SiN_x) single layers (50 nm thick) deposited by HWCVD with Ar plasma treatment between successive layers	20

Appendix A. ***Continued.***

Reactor Type	Subs. Type	Subs. T (°C)	NH_3 Flow Rate (sccm)	SiH_4 Flow Rate (sccm)	H_2 Flow Rate (sccm)	Duration of Deposit. (sec)	Working Pressure (torr)	RF Power (W) or Power Density (W/cm^2)	Film Thick. (nm)	Post Deposition Treatment	Pertinent Details	Reference
CVD reactor with Ar wave plasma generated near the surface of a dielectric alumina window with a microwave frequency of 2.45 GHz Distance between alumina window and substrate stage set at 200 mm	25 μ-thick polyimide base substrates	90	500 (mixed with 350 sccm Ar)	70	None	360	75×10^{-3}	1.57 W/cm^2	50	None reported	Prior to deposition, polyimide base film was baked at 100°C for 30 min in a glove box with moisture and oxygen maintained at less than 0.1 ppm, then directly transferred from the glove box to the SWP-CVD system without exposure to the air.	23, 22
HW-CVD reactor with Ta filament Glow-discharge (PECVD) chamber for sequences of SiN_x single layers with Ar plasma surface treatment between individual layers deposition steps	PET substrates	100	varied	2	54	360	25×10^{-3}	0.35 W/cm^2 (for Ar plasma treatment @50 mTorr only)	50	None reported	For multilayered SiN_x depositions, samples transferred back and forth between HWCVD to PECVD chamber without breaking vacuum between deposition steps For Ar treatment, samples were clamped to top electrode and heated to 100°C and bottom electrode was RF-powered Optimal SiN_x growth conditions achieved by varying 3 parameters: Hydrogen dilution, ratio of NH_3 to SiH_4, and Ta filament current. Single and multi-layer SiN_x films grown (the latter with intermediate Ar plasma treatment steps)	20
Remote-controlled PE-CVD chamber	⟨100⟩ p-type Si substrates	300	varied (6.3 to 14 sccm)	14	N/A	1800	N/A	N/A	N/A	SiN_x samples transferred from PECVD to conventional furnace with vacuum break SiN_x films annealed in N_2 flow Annealing temperature: varied from 700–1100°C Annealing Duration: 30–60 mins	Excess Si in Si-rich SiN_x films controlled by varying the NH_3/ SiH_4 flow ratio between 0.45 to 1.0	32

Appendix A. ***Continued.***

Reactor Type	Subs. Type	Subs. T (°C)	NH_3 Flow Rate (sccm)	SiH_4 Flow Rate (sccm)	H_2 Flow Rate (sccm)	Duration of Deposit. (sec)	Working Pressure (torr)	RF Power (W) or Power Density (W/cm^2)	Film Thick. (nm)	Post Deposition Treatment	Pertinent Details	Reference
Low-pressure CVD standard reactor	p-type (100) Si substrates 5 nm-thick SiO_2 thin films on p-type (100) Si substrates	750	N/A	None $SiCl_2H_2$ used as Si source (flow rate: N/A)	None N_2 used (flow rate: N/A)	N/A	0.6	100	33–231	None reported	SiN_x films were deposited directly on a 5 nm-thick SiO_2 thin films on p-type (100) Si	77
PE-CVD standard chamber with a working frequency of 2.45 GHz	a-Si:H substrates	N/A	N/A	N/A	N/A	N/A	25×10^{-3}	1000	80	None reported	SiN_x films with refractive index of 1.5–1.8 were used as antireflection coating	78
PE-CVD Chamber	HF solution rinsed Si(100) wafers	200–400	N/A	N/A	N/A	N/A	0.6	100	100–500	None reported	RF Sputtered SiN_x films were of higher density than their PECVD counterparts	25
Linear microwave plasma batch processing system with a working frequency of 2.45 GHz Two deposition modes: Low total flow rate and high total flow rate	c-Si, UV cured acrylates and PEN substrates	100	Low total flow rate (400 sccm) R = SiH_4/NH_3 flow ratio = 0.05–0.5		None Ar used (flow rate: 200 sccm)	180–1020 secs	6×10^{-2}	1000 W/m^2	79–100	None reported	The films were a-SiN_x:H	79
		110	High total flow rate (600 sccm) R = SiH_4/NH_3 flow ratio = 0.05–0.5		None Ar used (flow rate: 200 sccm)	105–700 secs	8.5×10^{-2}	835 W/m^2	101–175	None reported	The films were a-SiN_x:H	
Standard PE-CVD chamber	N/A	N/A	N/A	N/A	N/A	N/A	N/A	N/A	N/A	None reported	Excellent reliability shown for vanadyl-phthalocyanine (VOPc) thin film transistors (TFTs) with SiN_x as gate insulator	33
Pulsed RF with a low frequency (200 Hz) square wave envelope PECVD chamber Pulsed-RF supply generated by modulating a continuous wave (CW) RF supply using the 200 Hz signal generator with 50% duty cycle	c-Si substrates	150	40	4	120	N/A	0.8	130 mW/cm^2	N/A	None reported	200 Hz modulation used to ensure that the duration of the off-cycle (2.5ms) is significantly shorter than the gas residence time (∼1s) and achieve a growth rate that is $\frac{1}{2}$ of that for CW-RF growth	34

Appendix A. *Continued.*

Reactor Type	Subs. Type	Subs. T (°C)	NH_3 Flow Rate (sccm)	SiH_4 Flow Rate (sccm)	H_2 Flow Rate (sccm)	Duration of Deposit. (sec)	Working Pressure (torr)	RF Power (W) or Power Density (W/cm^2)	Film Thick. (nm)	Post Deposition Treatment	Pertinent Details	Reference
Standard PE-CVD chamber	4-inch GaAs bare and device wafers	N/A	14–16	14	0	240–300	N/A	N/A	40–60	Rapid thermal annealing (RTA) in ambient consisting of: Ar only, Ar with 20% O2 and Ar with 50% O_2 RTA T: 850°C, 900°C, 950°C and 1050°C	Films consisted of Si nanometer size inclusions (Si-ni) in Si-rich SiN_x matrix	38
Standard PE-CVD chamber	p-doped (100) oriented Fz-wafers with a resistivity of 1 Ω-cm	200–400	N/A	N/A	N/A	N/A	N/A	N/A	N/A	SiN_x samples annealed at 830°C for better hydrogen passivation and reduced leakage current	CV measurements in crystalline solar cells showed that interfacial trap density and fixed charges are higher for PECVD SiN_x than thermal SiO_2 and PECVD SiO_2	36
Standard PE-CVD chamber	Oxidized ⟨111⟩ p-type Si substrates	300–340	(2% SiH_4 diluted in N_2) flow rate: 285 sccm	15	None	60–600	0.4	15 W	50	None reported	A high $(SiH_4{:}N_2)/NH_3$ flow ratio was employed in order to obtain high-refractive-index SiN_x film	24
Standard PE-CVD chamber	4-inch GaAs bare and device wafers	300	15	15	N_2 used As diluent gas	N/A	N/A	Comb. of both high frequency (HF) and low frequency (LF) power	50–70		Single and multilayered SiN_x films were deposited using the same processing parameters	16

Appendix B. Summary of SiN_x Sputtering Parameters and Post Processing Treatments.

Reactor Type	Subs. Type	Subs. T (°C)	Sputtering Gas Ar (sccm)	Sputtering Gas N_2 (sccm)	Duration of Deposit. (sec)	Working Pressure (torr)	Plasma Power (W) or Power Density (W/cm^2)	Film Thick. (nm)	Post Deposition Treatment	Pertinent Details	Reference
RF Magnetron Sputtering System	Double-side polished, single crystalline n-type (P doped) ⟨100⟩ CZ-Si wafers (ρ>50 Ωcm)	R.T.	Ar + N_2 mixture 20	60	N/A	2.25–6.75 × 10^{-3}	300–900 W (RF power density of 1.5–4.5 W/cm^2)	500	None reported	Pre-deposition Si wafer inverse sputter etching clean step in same reactor: Substrate temperature: N/A Sputtering gas: Ar Ar flow rate: 20 sccm N_2 flow rate: 0 sccm RF Power: 200W Working Pressure: 4.0 × 10^{-3} torr	116
DC Magnetron Sputtering System (same as one used for RF sputtering above)	Double-side polished, single crystalline n-type (P doped) ⟨100⟩ CZ-Si wafers (ρ > 50 Ωcm)	R.T.	None Used	60		2.25–6.75 × 10^{-3}	300–900W (DC power density of 1.5–4.5 W/cm^2)	500	None reported	Pre-deposition Si wafer inverse sputter etching clean step in same reactor: Substrate temperature: N/A Sputtering gas: Ar Ar flow rate: N/A N_2 flow rate: 0 sccm DC Power: 200W Working Pressure: ∼4.0 × 10^{-3} torr	74
RF Magnetron Sputtering Reactor	p-type (100) Si substrates (ρ = 15 Ωcm)	500	Ar + N_2 mixture N/A	N/A	N/A	N/A	N/A	3	Half of the samples annealed at 800°C for 15s in continuous N_2 flow	The RMS SiN_x films were deposited on p-type Si with x = 0.8 (Si-rich SiN_x)	75
Standard RMS Reactor	Hydrofluoric acid (HF) solution rinsed Si(100) wafers	R.T. to 300	Ar + N_2 mixture		N/A	N/A	50	100–500	None reported	RF Sputtered SiN_x films were of higher density than their PECVD counterparts	25
Magnetron co-sputtering system @ 5 × 10^{-7} base pressure Two targets used: Si and SiN_x	Si wafers and quartz slides	R.T.	N/A	0	N/A	1.5 × 10^{-2}	50 W (SiN_x target RF power) 6 W (Si target DC power	5 nm (Si-rich SiN_x) and 1 nm (SiN_x)	Samples annealed in conventional quartz-tube furnace for 1 h at 900, 1000 and 1100°C in N_2	Films consisted of 25 alternating layers of Si-rich SiN_x and 1 nm SiN_x Films capped with a sputtered SiN_x capping layer of ∼10 nm to prevent moisture and oxidation during thermal annealing	31

Appendix C. Summary of SiN_x Atomic Layer Deposition Parameters and Post Processing Treatments.

Reactor Type	Subs. Type	Subs. T (°C)	Si Source (Vapor* Pressure. torr)	Si Source Pulse Exposure	N Source (flow rate)	N Source Pulse Duration (sec)	Purge Gas	Purge Pulse Duration (sec)	Plasma Type	Working Pressure (torr)	Film Thick. (nm)	Pertinent Details	Reference
Thermal ALD reactor	Insulators (e.g., SiO_2, HfO_2); conductor; semi-conductors	175–250	SiI_4 (N/A)	N/A	NH_3 or t-butyl hydrazine ($C_4H_{12}N_2$)	N/A	He, Ar, or N_2	N/A	None	0.1–1.0	1.3 per cycle	—-	100
PE-ALD in a hot-wall reactor	Single crystal Si (100) wafers	350	3DMAS 7.1 @R.T.	0.4s	N_2 (40 sccm)	15.0	Ar	10	Remote ICP plasma (300 W @ 13.56 MHz)	0.4	~12	3 h, in-situ, remote plasma post-treatment in H_2 @ flow rate of 100 sccm and plasma pressure of H_2 mixed with Ar of 300 mTorr (@substrate temperature of 350°C) to remove residual carbon	80
Hot-wall reactor and cold-wall reactor	Single crystal Si (100) wafers	350	3DMAS, TSA, DCS	Varied function of Si source	NH_3 or H_2 + N_2 plasma	15	N_2	3	Remote ICP plasma(300 W @ 13.56 MHz for hot-wall reactor and 400 W for cold-wall reactor)	N/A	12	In-cycle and post-deposition plasma processing inside the PE-ALD reactor were employed to increase film density	81
Traveling-wave-type cold-wall reactor	β-Si_3N_4	300	HCDS	1 torr.s – 50 torr.s	NH_3	10^3 torr.s	Ar	N/A	Remote ICP plasma (100W @ 13.56 MHz)	1.5	N/A	Films used for ab initio density functional theory calculations of the reactivity of different β-Si_3N_4 surface sites with $SiCl_4$ and Si_2Cl_6 precursors	82
Traveling-wave-type cold-wall reactor	N/A	200–500	DTDN2-H2 1.0@60°C	3.0s	N_2	12.0	N_2	16s	Remote ICP plasma 100W @ 13.56 MHz	N/A	~16.5	Energies of adsorption and reaction of DTDN2-H2 with SiN_x surface were also calculated by density functional theory	83

Appendix C. ***Continued.***

Reactor Type	Subs. Type	Subs. T (°C)	Si Source (Vapor Pressure. torr)	Si Source Pulse Exposure	N Source (flow rate)	N Source Pulse Duration (sec)	Purge Gas	Purge Pulse Duration (sec)	Plasma Type	Working Pressure (torr)	Film Thick. (nm)	Pertinent Details	Reference
Capacitively coupled plasma reactor	Si	325	BDEAS, TEAS, TIPAS, DIPAS	N/A	NH_3	N/A	Ar	N/A	Direct capacitively coupled plasma (CCP) 100–300 W @ 13.56 MHz	3	∼1.5–1.8	Additional plasma steps were employed after Si precursor purge to improve efficiency of precursor adsorption and lower deposition temperature	84
Direct plasma reactor	Si (100) wafers	250–300	NPS	1.0s	Direct N_2 plasma	2–30	Ar	15	Direct plasma @ 13.56 MHz	0.56	0.14 per cycle	ALD SiN_x from TSA was used for comparison	85
Thermal ALD reactor	Si, SiO_2, strained Si, Si on insulator (SOI), GaAs, Ge, metals, SiN_x	350–600°C	Si halides containing Br and/or I halogens (e.g., SiI_4, $SiBr_4$, $SiBr_{4-x}I_x$ (x = 1–3); Si_yX_{2y+2} (y > 2, and X is one or more Br or I)	∼5.0	N-containing reactant (e.g., NH_3)	∼30.0	Ar	20.0	Thermal	N/A	∼8.0	Substrate exposure to Ar plasma prior to SiN_x ALD led to significantly lower SiN_x wet etch rates	86
Thermal ALD reactor	p-type Si wafers	310–500	OCTS	2–15	NH_3	2–30	N/A	15 @ 500 sccm	N/A	0.7	15–35	SiN_x films deposited in ALD mode using 600 deposition cycles Film thickness controlled by deposition temperature	87

Appendix C. ***Continued.***

Reactor Type	Subs. Type	Subs. T (°C)	Si Source (Vapor Pressure. torr)	Si Source Pulse Exposure	N Source (flow rate)	N Source Pulse Duration (sec)	Purge Gas	Purge Pulse Duration (sec)	Plasma Type	Working Pressure (torr)	Film Thick. (nm)	Pertinent Details	Reference
Remote PA-ALD reactor	ZnSe internal reflection crystal (IRC)	350–450	HCDS	5–30	NH_3 plasma	5–45	Ar	30 @ 100 sccm	NH_3	0.7–1	30	Surface reactions during Si_2Cl_6 and NH3 plasma half-cycles were observed using in situ attenuated total reflection FTIR to identify surface reactive sites, and elucidate H incorporation mechanism in SiN_x	88
Remote PA-ALD reactor	c-Si with thin oxide layer	R.T.-500	BTBAS	0.15–3.0	N_2	10	Ar	1 @ 100 sccm	Remote ICP plasma 600 W @ 13.56 MHz	10^{-6}	N/A	Properties dependent on plasma exposure time, pressure and substrate temperature	89
Remote PA-ALD reactor	N/A	N/A	BTBAS	N/A	NH_3 or N_2 $H_2 + N_2$ plasma	N/A	N/A	N/A	N/A	N/A	N/A	Comparison of the effects of NH_3, N_2, or $H_2 + N_2$ plasma on SiN_x growth rates	90
Remote Plasma reactor	c-Si with thin oxide layer	80–200	BTBAS	0.15–3.0	N_2	10	Ar		Remote ICP plasma 600 W @ 13.56 MHz	0.8	10	Thin films of SiN_x deposited at low temperatures	91
Remote PA-ALD reactor	N/A	200–400	BTBAS	0.15–3.0	N_2	10	Ar	10 @ 100 sccm	Remote ICP plasma 600 W @ 13.56 MHz	0.2–0.4		Re-deposition controlled by gas residence time during the plasma step	89

Appendix C. ***Continued.***

Reactor Type	Subs. Type	Subs. T (°C)	Si Source (Vapor Pressure. torr)	Si Source Pulse Exposure	N Source (flow rate)	N Source Pulse Duration (sec)	Purge Gas	Purge Pulse Duration (sec)	Plasma Type	Working Pressure (torr)	Film Thick. (nm)	Pertinent Details	Reference
Direct plasma reactor	Poly-Si/TiN/HfO_2 stacks	400 or 500	DCS, MCS	N/A	Ionized NH_3	N/A	N/A	N/A	Direct plasma	N/A	<5 nm	DCS used for SiN_x for gate encapsulation applications @500°C; MCS used for SiN_x for spacer applications @400°C	93
Remote PA-ALD reactor	p-type Si (100)	50–400	TSA @ 12°C (315 torr @R.T.)	0.2	NH_3	5	Ar	15	Remote plasma 100W@ 13.56 MHz	0.3	4–25	SiN_x thin film characteristics controlled by dep. temp. to adjust the defect density for charge trap flash memory applications	94
Thermal ALD reactor	Bare β-Si_3N_4 surface	N/A	BDEAS, BTBAS	N/A	NH_3	N/A	N/A	N/A	N/A	N/A	N/A	First principles study using density functional theory to model the growth of a Si_3N_4 surface in a full ALD cycle	95
Thermal or plasma ALD reactor	(100) double-sided Si	450	Dialkylamide silanes with formula SiH_2 $(NR'R'')_2$ including: SiH_2DMA_2[R=R″=CH_3]; bis-(dimethylamino)silane, SiH_2HFMA_2 [R=R″=CF_3]; bis-(hexa-fluorodimethylamino)silane], SiH_2EMA_2 [R′=CH_3,R″+=CH_2CH_3]; bis(ethylmethylamino)silane], BDEAS, BTBAS, $SiH_2(NH_2)_2$ (diaminosilane); and DIPAS SiH_2Cl_2 (dichlorosilane); $SiH_2(CH_3)_2$ (dimethylsilane) and SiH_4	~1.0–8.0 torr.sec	NH_3	N/A	N/A	N/A	N/A	N/A	N/A	First-principles density functional theory to probe differences between ALD O_2 and Si_3N_4 using various theoretical approaches, including model reaction pathways, acidity/basicity of the oxide vs nitride surfaces and overall energetics as a function of precursor functional group	96

Appendix C. ***Continued.***

Reactor Type	Subs. Type	Subs. T (°C)	Si Source (Vapor Pressure. torr)	Si Source Pulse Exposure	N Source (flow rate)	N Source Pulse Duration	Purge Gas	Purge Pulse Duration (sec)	Plasma Type	Working Pressure (torr)	Film Thick. (nm)	Pertinent Details	Reference
Thermal or PE-ALD reactor	Si structures	400	Si precursors containing an iodine ligand such as $HSiI_3$, H_2SiI_2, H_3SiI, $H_2Si_2I_4$, $H_4Si_2I_2$, H_5Si_2I)	0.05–5.0	NH_3, N_2H_4, N_2	0.1–10	N_2, Ar or He	0.1–10	Remote or direct plasma @10–1000 W	N/A	N/A	SiNx films exhibited etch rates in diluted HF that were half of those for SiO_2	101
Parallel –plate capacitance PE-ALD reactor	(100) double-sided polished Si with native SiO_2 layer	400	SiH_4	0.0–15.0	N_2	0.5–90	N_2	1–5	Low frequency (LF) (200–400 kHz) and high frequency (HF) (13.56 MHz) power sources	2.5	∼0.5–90	PEALD SiN_x:H growth was performed both on native SiO_2 and on 25 nm PECVD SiN_x:H and SiO_2 films previously deposited on native oxide of the Si substrate	11
PE-ALD reactor	SiO_2 substrates	270°C	TIPAS	0.5–2.0	NH_3	8.0	Ar	10.0	Direct 13.56 MHz plasma @100W	3		PE-ALD SiN_x was part of forming $RuSiN_x$ films as diffusion barrier for Cu interconnects	97,98
Thermal in traveling-wave-type cold-wall reactor)	B-doped Si (100) wafers	∼515–573°C	HCDS	0.1–3.0 × 10^8L	NH_3	1.0–10 × 10^8L	Ar	N/A	No plasma	1 torr and 10 torr	20	SiN_x films were nonstoichiometric and easily oxidized by air exposure to contain 7–8 at.% oxygen	117

*For full descriptions of Si source acronyms used in this Appendix, see Table V.

References

1. W. Daves, A. Krauss, N. Behnel, V. Häublein, A. Bauer, and L. Frey, *Thin Solid Films*, **519**(18), 5892 (2011).
2. P. Kouakou, M. Belmahi, V. Brien, V. Hody, H. N. Migeon, and J. Bougdira, *Surf. Coat. Technol.*, **203**(3–4), 277 (2008).
3. A. S. Bhattacharyya and S. K. Mishra, *J. Raman Spectrosc.*, **41**(10), 1234 (2010).
4. V. I. Ivashchenko, A. O. Kozak, O. K. Porada, L. A. Ivashchenko, O. K. Sinelnichenko, O. S. Lytvyn, T. V. Tomila, and V. J. Malakhov, *Thin Solid Films*, **569**, 57 (2014).
5. T. Lube and J. Dusza, *J. Eur. Ceram. Soc.*, **27**(2–3), 1203 (2007).
6. H. Matsumura, *Japanese J. Appl. Physics, Part 1 Regul. Pap. Short Notes Rev. Pap.*, **37**(6 A), 3175 (1998).
7. N. I. Fainer and V. I. Kosyakov, *J. Struct. Chem.*, **56**(1), 163 (2015).
8. C. Zhuang, R. Fuchs, C. Schlemper, T. Staedler, and X. Jiang, *Thin Solid Films*, **592**, 167 (2015).
9. Y. Awad, M. A. El Khakani, C. Aktik, J. Mouine, N. Camiré, M. Lessard, and M. Scarlete, *Mater. Chem. Phys.*, **104**(2–3), 350 (2007).
10. E. Graef, B. Huizing, and R. Mahnkopf, *International Technology Roadmap for Semiconductors 2.0*, 2015th ed., 2015.
11. S. W. King, *J. Vac. Sci. Technol. A*, **29**(4), 41501 (2011).
12. S. W. King, *ECS J. Solid State Sci. Technol.*, **4**(1), N3029 (2014).
13. X. Meng, Y. -C. Byun, H. Kim, J. Lee, A. Lucero, L. Cheng, and J. Kim, *Materials (Basel).*, **9**(12), 1007 (2016).
14. T. Usami, T. Ide, Y. Kakuhara, Y. Ajima, K. Ueno, T. Maruyama, Y. Yu, E. Apen, K. Chattopadhyay, B. Van Schravendijk, N. Oda, and M. Sekine, In *2006 International Interconnect Technology Conference*, IITC; IEEE, 2006; pp 125.
15. Y. Kuo, *Vacuum*, **51**(4), 741 (1998).
16. J. Yota, *ECS Trans.*, **35**(4), 229 (2011).
17. W. Liao, X. Zeng, W. Yao, and X. Wen, *Appl. Surf. Sci.*, **351**, 1053 (2015).
18. T. Stapinski and B. Swatowska, *J. Electron. Mater.*, **37**(6), 905 (2008).
19. Z. Khatami, P. R. J. Wilson, J. Wojcik, and P. Mascher, *Thin Solid Films*, **622**, 1 (2017).
20. S. Majee, M. F. Cerqueira, D. Tondelier, J. C. Vanel, B. Geffroy, Y. Bonnassieux, P. Alpuim, and J. E. Bourée, *Thin Solid Films*, **575**, 72 (2015).
21. P. Alpuim, S. Majee, M. F. Cerqueira, D. Tondelier, B. Geffroy, Y. Bonnassieux, and J. E. Bourée, *Thin Solid Films*, **595**, 258 (2015).
22. S. Ueno, Y. Konishi, and K. Azuma, *Thin Solid Films*, **580**, 116 (2015).
23. K. Azuma, S. Ueno, Y. Konishi, and K. Takahashi, *Thin Solid Films*, **580**, 111 (2015).
24. M. Smietana, W. J. Bock, and J. Szmidt, *Thin Solid Films*, **519**(19), 6339 (2011).
25. M. B. Takeyama, M. Sato, Y. Nakata, Y. Kobayashi, T. Nakamura, and A. Noya, *Jpn. J. Appl. Phys.*, **53**, 19 (2014).
26. J. S. Lee, B. B. Sahu, and J. G. Han, *Phys. Chem. Chem. Phys.*, **18**(47), 32198 (2016).
27. N. Tabassum, V. Nikas, B. Ford, M. Huang, A. E. Kaloyeros, and S. Gallis, *Appl. Phys. Lett.*, **109**(4), 43104 (2016).
28. V. Nikas, N. Tabassum, B. Ford, L. Smith, A. E. Kaloyeros, and S. Gallis, *J. Mater. Res.*, (30), 1 (2015).
29. S. Gallis, V. Nikas, E. Eisenbraun, M. Huang, and A. E. Kaloyeros, *J. Mater. Res.*, **24**(8), 2561 (2009).
30. S. Gallis, M. Huang, and A. E. Kaloyeros, *Appl. Phys. Lett.*, **90**(16), 161914 (2007).
31. Y. H. So, S. Huang, G. Conibeer, and M. A. Green, *Thin Solid Films*, **519**(16), 5408 (2011).
32. T. V. Torchynska, J. L. Casas Espinola, E. Vergara Hernandez, L. Khomenkova, F. Delachat, and A. Slaoui, *Thin Solid Films*, **581**, 65 (2015).
33. L. Wang, H. Qin, W. Zhang, L. Zhang, and D. Yan, *Thin Solid Films*, **545**, 514 (2013).
34. A. Ahnood, Y. Suzuki, A. Madan, and A. Nathan, *Thin Solid Films*, **520**(15), 4831 (2012).
35. T. Chen, Y. Huang, D. Yang, R. Carius, and F. Finger, *Thin Solid Films*, **519**(14), 4523 (2011).
36. J. M. Kopfer, S. Keipert-Colberg, and D. Borchert, *Thin Solid Films*, **519**(19), 6525 (2011).
37. M. S. Bailly, J. Karas, H. Jain, W. J. Dauksher, and S. Bowden, *Thin Solid Films*, **612**, 243 (2016).
38. A. S. Keita, A. En Naciri, F. Delachat, M. Carrada, G. Ferblantier, A. Slaoui, and M. Stchakovsky, *Thin Solid Films*, **519**(9), 2870 (2011).
39. J. Wei, P. L. Ong, F. E. H. Tay, and C. Iliescu, *Thin Solid Films*, **516**(16), 5181 (2008).
40. D. Fine, A. Grattoni, R. Goodall, S. S. Bansal, C. Chiappini, S. Hosali, A. L. van de Ven, S. Srinivasan, X. Liu, B. Godin, L. Brousseau, I. K. Yazdi, J. Fernandez-Moure, E. Tasciotti, H. J. Wu, Y. Hu, S. Klemm, and M. Ferrari, *Adv. Healthc. Mater.*, **2**(5), 632 (2013).
41. J. M. Maloney, S. A. Lipka, S. P. Baldwin, H. Hämmerle, K. Kobuch, K. Kohler, W. Nisch, H. Sachs, M. Stelzle, Y. Li, R. S. Shawgo, B. Tyler, P. T. Henderson, J. S. Vogel, A. Rosenberg, P. B. Storm, R. Langer, H. Brem, M. J. Cima, D. J. Edell, J. W. Osenbach, M. Vogt, R. Hauptmann, G. Schmitt, J. -W. Schultze, F. Faßbender, G. Buß, H. Lüth, and M. Schöning, *MRS Online Proc. Libr. Arch.*, **872**(3), 797 (2005).
42. G. Kotzar, M. Freas, P. Abel, A. Fleischman, S. Roy, C. Zorman, J. M. Moran, and J. Melzak, *Biomaterials*, **23**(13), 2737 (2002).
43. A. Neumann, T. Reske, M. Held, K. Jahnke, C. Rago, and H. R. Maier, *J. Mater. Sci. Mater. Med.*, **15**(10), 1135 (2004).
44. C. C. Guedes E Silva, B. König, M. J. Carbonari, M. Yoshimoto, S. Allegrini, and J. C. Bressiani, *J. Biomed. Mater. Res. - Part A*, **84**(2), 337 (2008).
45. T. J. Webster, A. A. Patel, M. N. Rahaman, and B. Sonny Bal, *Acta Biomater.*, **8**(12), 4447 (2012).
46. M. R. Badaruddin, M. R. Muhamad, and S. A. Rahman, *Thin Solid Films*, **519**(15), 5082 (2011).
47. M. Belmahi, S. Bulou, A. Thouvenin, L. De Poucques, R. Hugon, L. Le Brizoual, P. Miska, D. Genève, J. L. Vasseur, and J. Bougdira, *Plasma Process. Polym.*, **11**(6), 551 (2014).
48. Z. Ma, J. Zhou, Z. Chen, and E. Xie, *Diam. Relat. Mater.*, **20**(4), 475 (2011).
49. S. Bulou, L. Brizoual, P. Le Miska, L. Poucques, R. de Hugon, and M. Belmahi, *IOP Conf. Ser. Mater. Sci. Eng.*, **12**(1), 12002 (2010).
50. A. K. Sinha and E. Lugujjo, *Appl. Phys. Lett.*, **32**(4), 245 (1978).
51. E. F. Krimmel and R. Hezel, *Silicon Nitride in Microelectronics and Solar Cells (Gmelin Si B 5c)*, A. Peble and F. Schröder, Eds., Springer Berlin Heidelberg: Berlin, Heidelberg, 1991.
52. F. I. Riley, *J. Am. Ceram. Soc.*, **83**(2), 245 (2000).
53. S. Hampshire, *J. Achiev. Mater. Manuf. Eng.*, **24**(1), 43 (2007).
54. G. Ziegler, J. Heinrich, and G. Wötting, *J. Mater. Sci.*, **22**(9), 3041 (1987).
55. Y. Kaga, H. Imamura, and J. Watanabe, Silicon nitride substrate manufacturing method, silicon nitride substrate, silicon nitride circuit substrate, and semiconductor module. 8,858,865, (2014).
56. M. Weinmann, In *Inorganic Polymers*, R. Jaeger M. De Gleria, Eds., Nova Science Publishers, 2007; pp 371.
57. G. Mera, M. Gallei, S. Bernard, and E. Ionescu, *Nanomaterials*, **5**(2), 468 (2015).
58. E. Kroke, Y. Li, C. Konetschny, E. Lecomte, C. Fasel, and R. Riedel, *Mater. Sci. Eng. R Reports*, **26**(4–6), 97 (2000).
59. A. L. Hector, *Coord. Chem. Rev.*, **323**, 120 (2016).
60. G. Barroso, Q. Li, G. Motz, and R. K. Bordia, *Am. Ceram. Soc. Bull.*, **96**(3), 42 (2017).
61. D. Seyferth and G. H. Wiseman, *J. Am. Ceram. Soc.*, **67**(7), C132 (1984).
62. B. Arkles, *J. Electrochem. Soc.*, **133**(1), 233 (1986).
63. L. A. Liew, W. Zhang, V. M. Bright, L. An, M. L. Dunn, and R. Raj, *Sensors Actuators, A Phys.*, **89**(1–2), 64 (2001).
64. A. Lukacs, *Am. Ceram. Soc. Bull.*, **86**(1), 9301 (2007).
65. N. Shinde, Y. Takano, J. Sagan, V. Monreal, and T. Nagahara, *J. Photopolym. Sci. Technol.*, **23**(2), 225 (2010).
66. T. Isoda, H. Kaya, H. Nishii, O. Funayama, T. Suzuki, and Y. Tashiro, *J. Inorg. Organomet. Polym.*, **2**(1), 151 (1992).
67. J. H. Lee, J. H. Cho, J. S. Choi, and D. Lee, Spin-on glass composition and method of forming silicon oxide layer in semiconductor manufacturing process using the same. US20040224537 A1, (2004).
68. B. C. Arkles, Y. Pan, and F. Jove, Hydridosilapyrroles, hydridosilaazapyrroles, thiasilacyclopentanes, method for preparation thereof, and reaction products therefrom. WO2016205073 A1, (2016).
69. A. Markwitz, H. Baumann, E. Krimmel, M. Rose, K. Bethge, P. Misaelides, and S. Logothetidis, *Vacuum*, **44**(3–4), 367 (1993).
70. B. Arkles, Y. Pan, and A. E. Kaloyeros, *Electrochem. Soc. Trans.*, **64**(9), 243 (2014).
71. L. Ju, N. C. Strandwitz, and M. Green, *J. Mater. Chem. C*, **4**(18), 4034 (2016).
72. S. M. George, *Chem. Rev.*, **110**(1), 111 (2010).
73. E. Eisenbraun, A. Upham, R. Dash, W. Zeng, J. Hoefnagels, S. Lane, D. Anjum, K. Dovidenko, A. Kaloyeros, B. Arkles, and J. J. Sullivan, *J. Vac. Sci. Technol. B Microelectron. Nanom. Struct.*, **18**(4), 2011 (2000).
74. D. Dergez, M. Schneider, A. Bittner, and U. Schmid, *Thin Solid Films*, **589**, 227 (2015).
75. L. Khomenkova, P. Normand, F. Gourbilleau, A. Slaoui, and C. Bonafos, *Thin Solid Films*, **617**, 143 (2016).
76. M. Śmietana, M. Dominik, M. Myśliwiec, N. Kwietniewski, P. Mikulic, B. S. Witkowski, and W. J. Bock, *Thin Solid Films*, **603**, 8 (2016).
77. K. Kobayashi, A. Suzuki, and K. Ishikawa, *Thin Solid Films*, **550**, 545 (2014).
78. D. Li, T. Kunz, N. Wolf, J. P. Liebig, S. Wittmann, T. Ahmad, M. T. Hessmann, R. Auer, M. Göken, and C. J. Brabec, *Thin Solid Films*, **583**(1), 25 (2015).
79. F. J. H. Van Assche, S. Unnikrishnan, J. J. Michels, A. M. B. Van Mol, P. Van De Weijer, M. C. M. Van De Sanden, and M. Creatore, *Thin Solid Films*, **558**, 54 (2014).
80. Y. Kim, J. Provine, S. P. Walch, J. Park, W. Phuthong, A. L. Dadlani, H. J. Kim, P. Schindler, K. Kim, and F. B. Prinz, *ACS Appl. Mater. Interfaces*, **8**(27), 17599 (2016).
81. J. Provine, P. Schindler, Y. Kim, S. P. Walch, H. J. Kim, K. H. Kim, and F. B. Prinz, *AIP Adv.*, **6**(6) (2016).
82. L. L. Yusup, J.-M. Park, Y.-H. Noh, S.-J. Kim, W.-J. Lee, S. Park, and Y.-K. Kwon, *RSC Adv.*, **6**(72), 68515 (2016).
83. J.-M. Park, S. J. Jang, L. L. Yusup, W.-J. Lee, and S.-I. Lee, *ACS Appl. Mater. Interfaces*, **8**(32), 20865 (2016).
84. S. Suh, S. W. Ryu, S. Cho, J.-R. Kim, S. Kim, C. S. Hwang, and H. J. Kim, *J. Vac. Sci. Technol. A Vacuum, Surfaces, Film.*, **34**(1), 01A136 (2016).
85. S. Weeks, G. Nowling, N. Fuchigami, M. Bowes, and K. Littau, *J. Vac. Sci. Technol. A Vacuum, Surfaces, Film.*, **34**(1), 01A140 (2016).
86. M. Saly, Deposition Of Si-H Free Silicon Nitride. US20160307748 A1, (2016).
87. S. Riedel, J. Sundqvist, and T. Gumprecht, *Thin Solid Films*, **577**, 114 (2015).
88. R. a. Ovanesyan, D. M. Hausmann, and S. Agarwal, *ACS Appl. Mater. Interfaces*, **7**(20), 10806 (2015).
89. H. C. M. Knoops, E. M. J. Braeken, K. de Peuter, S. E. Potts, S. Haukka, V. Pore, and W. M. M. Kessels, *ACS Appl. Mater. Interfaces*, **7**(35), 19857 (2015).
90. C. K. Ande, H. C. M. Knoops, K. de Peuter, M. van Drunen, S. D. Elliott, and W. M. M. Kessels, *J. Phys. Chem. Lett.*, **6**(18), 3610 (2015).

91. A. M. Andringa, A. Perrotta, K. De Peuter, H. C. M. Knoops, W. M. M. Kessels, and M. Creatore, *ACS Appl. Mater. Interfaces*, **7**(40), 22525 (2015).
92. H. C. M. Knoops, K. De Peuter, and W. M. M. Kessels, *Appl. Phys. Lett.*, **107**(1) (2015).
93. F. Koehler, D. H. Triyoso, I. Hussain, B. Antonioli, and K. Hempel, *Phys. Status Solidi Curr. Top. Solid State Phys.*, **11**(1), 73 (2014).
94. W. Jang, H. Jeon, C. Kang, H. Song, J. Park, H. Kim, H. Seo, M. Leskela, and H. Jeon, *Phys. Status Solidi*, **211**(9), 2166 (2014).
95. L. Huang, B. Han, B. Han, A. Derecskei-Kovacs, M. Xiao, X. Lei, M. L. O'Neill, R. M. Pearlstein, H. Chandra, and H. Cheng, *Phys. Chem. Chem. Phys.*, **16**(34), 18501 (2014).
96. C. A. Murray, S. D. Elliott, D. Hausmann, J. Henri, and A. LaVoie, *ACS Appl. Mater. Interfaces*, **6**, 10534 (2014).
97. T.-K. Eom, S.-H. Kim, D.-H. Kang, and H. Kim, *J. Electrochem. Soc.*, **158**(11), D657 (2011).
98. T.-K. Eom, S.-H. Kim, K.-S. Park, S. Kim, and H. Kim, *Electrochem. Solid-State Lett.*, **14**(1), D10 (2011).
99. K. Park, W. D. Yun, B. J. Choi, H. Kim, W. J. Do Lee, S. K. Rha, and C. O. Park, *Thin Solid Films*, **517**(14), 3975 (2009).
100. T. Saito, T. Nishizawa, Y. Kinoshita, and N. Nashida, Electronic component and manufacturing method for electronic component. US Pat. 9355987, (2016).
101. A. J. Niskanen, S. Chen, V. Pore, A. Fukazawa, and H. Fukuda, Si Precurosors for Deposition of SiN at Low Temperatures. US20140273531 A1, (2014).
102. R. Walsh, In *Silicon Compounds: Silanes and Silicones*, B. Arkles and G. L. Larson, Eds., 2008; pp 200.
103. J. A. Pople and L. A. Curtiss, *J. Chem. Phys.*, **95**(6), 4385 (1991).
104. B. Arkles and G. L. Larson, *Silicon Compounds: Silanes and Silicones*, 4th ed., 2013.
105. B. C. Arkles and A. E. Kaloyeros, Silicon based films formed from iodosilane precursors and method of making the same. US Pat. 6586056, (2003).
106. X. Lin, D. Endisch, X. Chen, and A. Kaloyeros, *MRS Proc.*, **495**, 107 (1997).
107. L. -Q. Xia and M. In Chang, *Handbook of Semiconductor Manufacturing Technology*, CRC Press, 2008; pp 13-1-13–87.
108. S. Koseki and A. Ishitani, *J. Appl. Phys.*, **72**(12), 5808 (1992).
109. D. L. Smith, A. S. Alimonda, and F. J. von Preissig, *J. Electrochem. Soc.*, **8**(3), 551 (1990).
110. D. L. Smith, A. S. Alimonda, C. Chen, S. E. Ready, and B. Wacker, *J. Electrochem. Soc.*, **137**(2), 614 (1990).
111. J. W. Smith, S. M. Seutter, and R. S. Iyer, *J. Electrochem. Soc.*, **152**(4), G316 (2005).
112. Y. Wu, H. Zhong, J. Romero, C. Tabery, C. Cheung, B. MacDonald, J. Bhakta, A. Halliyal, F. Cheung, and R. Ogle, *J. Electrochem. Soc.*, **150**(12), G785 (2003).
113. M. Tanaka, S. Saida, and Y. Tsunashima, *J. Electrochem. Soc.*, **147**(6), 2284 (2000).
114. K. E. Bean, P. S. Gleim, R. L. Yeakley, and W. R. Runyan, *J. Electrochem. Soc.*, **114**(7), 733 (1967).
115. S. M. Hu, *J. Electrochem. Soc.*, **113**(7), 693 (1966).
116. D. Dergez, M. Schneider, A. Bittner, N. Pawlak, and U. Schmid, *Thin Solid Films*, **606**, 7 (2016).
117. K. Park, W. D. Yun, B. J. Choi, H. Kim, W. J. Do Lee, S. K. Rha, and C. O. Park, *Thin Solid Films*, **517**(14), 3975 (2009).
118. L. Huang, B. Han, M. Fan, and H. Cheng, *RSC Adv.*, **7**(37), 22672 (2017).
119. L. Wang, R. W. Snidle, and L. Gu, *Wear.*, 159 (2000).
120. S. Schmidt, T. Hänninen, C. Goyenola, J. Wissting, J. Jensen, L. Hultman, N. Goebbels, M. Tobler, and H. Högberg, *ACS Appl. Mater. Interfaces*, **8**(31), 20385 (2016).
121. T. Serikawa and A. Okamoto, *J. Electrochem. Soc.*, **131**(12), 2928 (1984).
122. B. C. Joshi, G. Eranna, D. P. Runthala, B. B. Dixit, O. P. Wadhawan, and P. D. Vyas, *Indian J. Eng. Mater. Sci.*, **7**(5–6), 303 (2000).
123. T. S. Hickernell, F. M. Fliegel, and F. S. Hickernell, *IEEE Symp. Ultrason.*, 445 (1990).
124. M. Maeda and Y. Arita, *J. Appl. Phys.*, , **53**(10), 6852 (1982).
125. G. Carlotti, P. Colpani, D. Piccolo, S. Santucci, V. Senez, G. Socino, and L. Verdini, *Thin Solid Films*, **414**(1), 99 (2002).
126. F. S. Hickernell and T. S. Hickernell, *IEEE Trans. Ultrason. Ferroelectr. Freq. Control*, **42**(3), 410 (1995).
127. J. A. Taylor, *J. Vac. Sci. Technol. A Vacuum, Surfaces, Film.*, **9**(4), 2464 (1991).
128. S. King, R. Chu, G. Xu, and J. Huening, *Thin Solid Films*, **518**(17), 4898 (2010).
129. S. W. King and J. A. Gradner, *Microelectron. Reliab.*, **49**(7), 721 (2009).
130. J. J. Mei, H. Chen, W. Z. Shen, and H. F. W. Dekkers, *J. Appl. Phys.*, **100**(7), 73516 (2006).
131. M. Vila, D. Cáceres, and C. Prieto, *J. Appl. Phys.*, **94**(12), 7868 (2003).
132. Y. Toivola, J. Thurn, R. F. Cook, G. Cibuzar, and K. Roberts, *J. Appl. Phys.*, **94**(10), 6915 (2003).
133. Ferro-Ceramic Grinding Inc. Ceramic Silicon Nitride | Silicon Nitride Properties http://www.ferroceramic.com/silicon_nitride.htm (accessed Aug 20, 2017).
134. J. J. Vlassak and W. D. Nix, *J. Mater. Res.*, **7**(12), 3242 (1992).
135. P. French, P. Sarro, R. Mallée, E. Fakkeldij, and R. Wolffenbuttel, *Sensors Actuators A Phys.*, **58**(2), 149 (1997).
136. T. Kramer and O. Paul, *IEEE Sixt. Annu. Int. Conf. Micro Electro Mech. Syst.*, No. Mml, 678 (2003).
137. S. Hasegawa, Y. Amano, T. Inokuma, and Y. Kurata, *J. Appl. Phys.*, **72**(12), 5676 (1992).
138. V. Ziebart, O. Paul, U. Munch, and H. Baltes, *Mater. Res. Soc. Symp. - Proc.*, **505**(V), 27 (1998).
139. G. Ziegler, *Mater. Sci. Forum*, **47**, 162 (1989).
140. A. J. Eckel, *NASA Research News*, 2009, p https://web.archive.org/web/20090404161958.
141. C. H. Mastrangelo, Y. C. Tai, and R. S. Muller, *Sensors Actuators A. Phys.*, **23**(1–3), 856 (1990).
142. S. Govorkov, W. Ruderman, M. W. Horn, R. B. Goodman, and M. Rothschild, *Rev. Sci. Instrum.*, **68**(10), 3828 (1997).
143. A. J. Griffin, F. R. Brotzen, and P. J. Loos, *J. Appl. Phys.*, **76**(7), 4007 (1994).
144. R. Sultan, A. D. Avery, J. M. Underwood, S. J. Mason, D. Bassett, and B. L. Zink, *Phys. Rev. B*, **87**(21), 214305 (2013).
145. S. -M. Lee and D. G. Cahill, *J. Appl. Phys.*, **81**(6), 2590 (1997).
146. M. Bogner, A. Hofer, G. Benstetter, H. Gruber, and R. Y. Q. Fu, *Thin Solid Films*, **591**, 267 (2015).
147. A. Piccirillo and A. L. Gobbi, *J. Electrochem. Soc.*, **137**(12), 3910 (1990).
148. I. Khan and M. Zulfequar, *Mater. Sci. Appl.*, **2**(July), 738 (2011).
149. M. A. Signore, A. Sytchkova, D. Dimaio, A. Cappello, and A. Rizzo, *Opt. Mater. (Amst).*, **34**(4), 632 (2012).
150. E. A. Davis, N. Piggins, and S. C. Bayliss, *Solid State Phys.*, **20**(27), 4415 (1987).
151. A. J. Lowe, M. J. Powell, and S. R. Elliott, *J. Appl. Phys.*, **59**(4), 1251 (1986).
152. H. Charifi, A. Slaoui, J. P. Stoquert, H. Chaib, A. Hannour, and H. Charifi, *World J. Condens. Matter Phys.*, **6**(6), 7 (2016).
153. R. C. Dante and C. K. Kajdas, *Wear*, **288**, 27 (2012).
154. P. F. Carcia, R. S. McLean, M. H. Reilly, M. D. Groner, and S. M. George, *Appl. Phys. Lett.*, **89**(3), 31915 (2006).
155. D. S. Wuu, W. C. Lo, C. C. Chiang, H. B. Lin, L. S. Chang, R. H. Horng, C. L. Huang, and Y. J. Gao, *Surf. Coatings Technol.*, **197**(2–3), 253 (2005).